REVIEW

A Decade after Typhoon Morakot (2009): What Have We Learned about Its Physics and Predictability?

CHUNG-CHIEH WANG,[a] HUNG-CHI KUO,[b] YU-HAN CHEN,[b] SHIN-HAU CHEN,[a] AND KAZUHISA TSUBOKI[c]

[a] *Department of Earth Sciences, National Taiwan Normal University, Taipei, Taiwan*
[b] *Department of Atmospheric Sciences, National Taiwan University, Taipei, Taiwan*
[c] *Institute for Space-Earth Environmental Research, Nagoya University, Nagoya, Japan*

(Manuscript received 9 December 2021, in final form 21 August 2022)

ABSTRACT: Typhoon Morakot struck Taiwan during 7–9 August 2009 and became the deadliest tropical cyclone (TC) in five decades by producing up to 2635 mm of rain in 48 h, breaking the world record. The extreme rainfall of Morakot resulted from the strong interaction among several favorable factors that occurred simultaneously. These factors from large scale to small scale include the following: 1) weak environmental steering flow linked to the evolution of the monsoon gyre and consequently slow TC motion; 2) a strong moisture surge due to low-level southwesterly flow; 3) asymmetric rainfall and latent heating near southern Taiwan to further reduce the TC's forward motion as its center began moving away from Taiwan; 4) enhanced rainfall due to steep topography; 5) atypical structure with a weak inner core, enhancing its susceptibility to the latent heating effect; and 6) cell merger and back building inside the rainbands associated with the interaction between the low-level jet and convective updrafts. From a forecasting standpoint, the present-day convective-permitting or cloud-resolving regional models are capable of short-range predictions of the Morakot event starting from 6 August. At longer ranges beyond 3 days, larger uncertainty exists in the track forecast and an ensemble approach is necessary. Due to the large computational demand at the required high resolution, the time-lagged strategy is shown to be a feasible option to produce useful information on rainfall probabilities of the event.

KEYWORDS: Extreme events; Hurricanes/typhoons; Monsoons; Rainfall; Mesoscale forecasting; Numerical weather prediction/forecasting

1. Introduction

Due to its location in the paths of tropical cyclones (TCs) in the western North Pacific (WNP), Taiwan is struck by 3.6 typhoons per season (Wang 1989; Wu and Kuo 1999). Mainly due to the steep topography, in particular the Central Mountain Range (CMR) and the Snow Mountain Range (SMR; Fig. 1a), TCs can bring heavy to extreme rainfall amounts to Taiwan. Thus, flash floods, inundation, landslides, and debris flows constitute the major hazards from TCs in Taiwan. As the monsoon is also active in the WNP and East Asia (e.g., Ding and Chan 2005; Wang 2006; Zhou et al. 2011), extreme rainfall can occur when a TC interacts with the monsoon to enhance the moisture supply or lengthen the duration of heavy rainfall and thus the impacts from that rain.

In heavily populated, low-lying coastal regions around the world that encounter TCs, the gale-force winds and storm surge are major threats that cause great damage (Marks and Shay 1998; Emanuel 2005; Rogers et al. 2013). Some noteworthy examples are Cyclone Nargis (2008) in Myanmar (Webster 2008; McPhaden et al. 2009), Hurricanes Katrina (2005) and Sandy (2012) in the United States (e.g., McTaggart-Cowan et al. 2007; Blake et al. 2013; Galarneau et al. 2013), and Typhoon (TY) Haiyan (2013) in the Philippines (Soria et al. 2016). In Taiwan, such threats tend to occur only for intense TCs of particular track types, i.e., those TCs that approach Taiwan's low-lying plains from the southwest or move to a specific spot just to the northwest of the northern tip of the island. If the TCs do not make landfall, they maintain their strength and strong winds can blow directly onshore over flat low-lands. Because of these special conditions, TC-related wind damage events are less frequent in Taiwan. For most of the TCs that approach Taiwan from the east, the CMR contributes to increased rainfall on the windward side through uplifting (and decreased rainfall on the leeside), but the high terrain also reduces the TC intensity prior to and during landfall (e.g., Liou et al. 2016). Thus, in many circumstances, some areas, mainly the leeside, are protected from wind damage by the topography of Taiwan.

During 7–9 August 2009, Taiwan was hit by TY Morakot (2009), which became the deadliest TC on record since 1959, with casualties of nearly 700 [source: Central Weather Bureau (CWB) of Taiwan]. Reaching 2635 mm in 48 h (and 2855 mm in 4 days, Chanson 2010), the rainfall brought by Morakot broke many local records (Hsu et al. 2010; Wang et al. 2015). The high death toll in Taiwan was mainly caused by a single devastating landslide at around 0610 LST 9 August (LST = UTC + 8 h) that buried the entire village of Shiao-Lin, which is located in a

Denotes content that is immediately available upon publication as open access.

Corresponding author: Chung-Chieh Wang, cwang@ntnu.edu.tw

DOI: 10.1175/WAF-D-21-0197.1

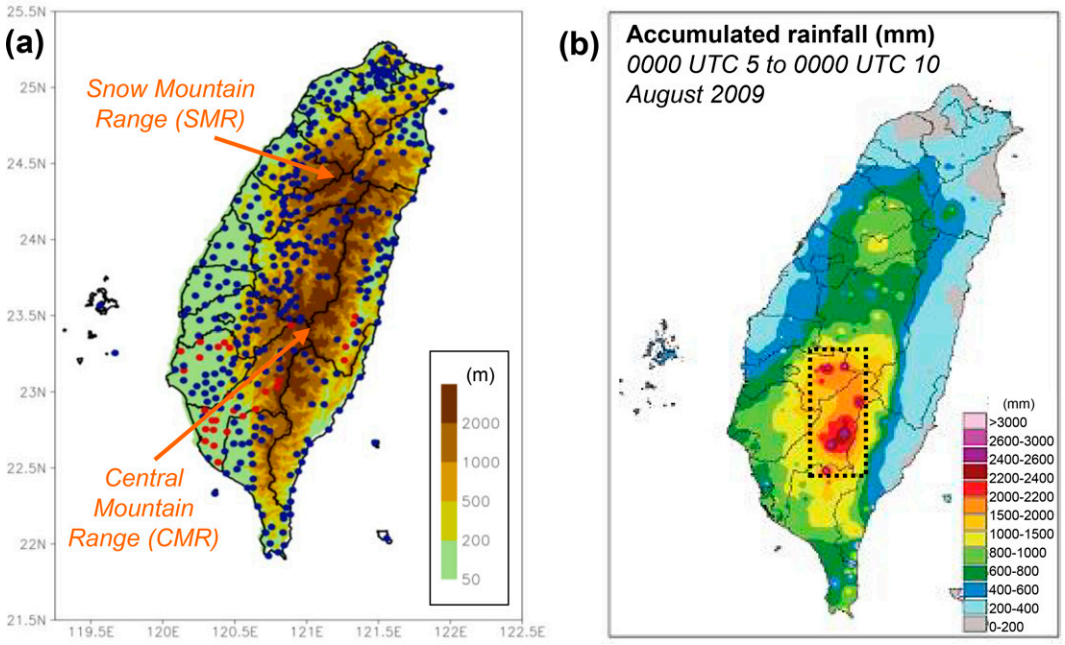

FIG. 1. (a) The topography (m; color) of Taiwan and the locations of rain gauges (dots) during TY Morakot (2009). The red dots depict those damaged by Morakot, and the two major mountain ranges CMR and SMR are marked. (b) Distribution of total (5 day) accumulated rainfall (mm) in Taiwan from 5 to 9 Aug 2009 [Source: Central Weather Bureau (CWB)]. The dotted box indicates the averaging region used in Fig. 9.

valley in the southern CMR. This landslide was due to the failure of a blockage that formed upstream earlier by mudslides from prolonged heavy rainfall (Petley 2010; C.-W. Chen et al. 2013; Wu et al. 2014). After Morakot, the Taiwan government launched a major effort to investigate the event and understand the reasons for its occurrence (Hsu et al. 2010; Lee et al. 2011; Wu 2013).

Approximately 75 papers have been published in the open literature on various aspects of TY Morakot (2009), including reviews by Hsu et al. (2010), Lee et al. (2011), and Wu (2013). In Lee et al. (2011), TY Morakot (2009) was termed a "perfect storm" due to its record-breaking rainfall in Taiwan (also Kuo et al. 2012). As the three reviews only referenced studies published up to 2011, it appears to be a suitable time now to provide a comprehensive review on TY Morakot (2009) in terms of what we have learned about the physical processes occurring on a variety of scales from large to small, and on the interactions across the scales. The first part of this review will be on the physics and dynamics of Morakot with particular emphasis on more unique or significant aspects of TY Morakot compared to more typical TCs in the Taiwan region.

The second part of the review is on the predictability of Morakot (2009) from the perspectives of numerical weather prediction and hazard reduction. First, a discussion is provided to answer the question whether the present-day models are capable of predicting the Morakot event? The answer is a resounding "yes." Then, an intercomparison of the setups and configurations of the numerical experiments will be used to isolate the model characteristics that contribute to the improved forecasts. A discussion on the reasons for the improvement are provided. Some modeling studies not focused on understanding the physical mechanisms are also reviewed in the second part of the paper. While attempting to be as comprehensive as possible, it is inevitable that some studies might be left out.

2. Review on the dynamics and physics of Morakot (2009): A perfect storm

For an extreme event like TY Morakot (2009), which was estimated by Chu et al. (2011) to have a return period of at least around 100 years for southwestern Taiwan, it is anticipated that a greater number of factors or ingredients must have interacted in a manner much more favorable than occurs with typical or ordinary TCs. Indeed, many studies have investigated these favorable factors ranging from large to small scales, including the interactions among them.

The infrared (IR) cloud imagery from the geostationary Multifunctional Transport Satellite (MTSAT) and the 850-hPa geopotential and wind fields from the National Centers for Environmental Prediction (NCEP) final analysis (FNL) at 1200 UTC 7 August 2009 are presented in Fig. 2. These analyses are about six hours before landfall in Taiwan, which is indicated by the best track from the CWB in Fig. 2a. After Morakot reached tropical storm (TS) intensity on 3 August, it moved almost due west to approach Taiwan but then turned toward the north-northwest during 7 August (Fig. 2a). Such a sudden change in track is typically accompanied by slow TC translation, as it indicates a shift in the large-scale steering flow (Wu et al. 2011; Chien and Kuo 2011). For TY Morakot (2009),

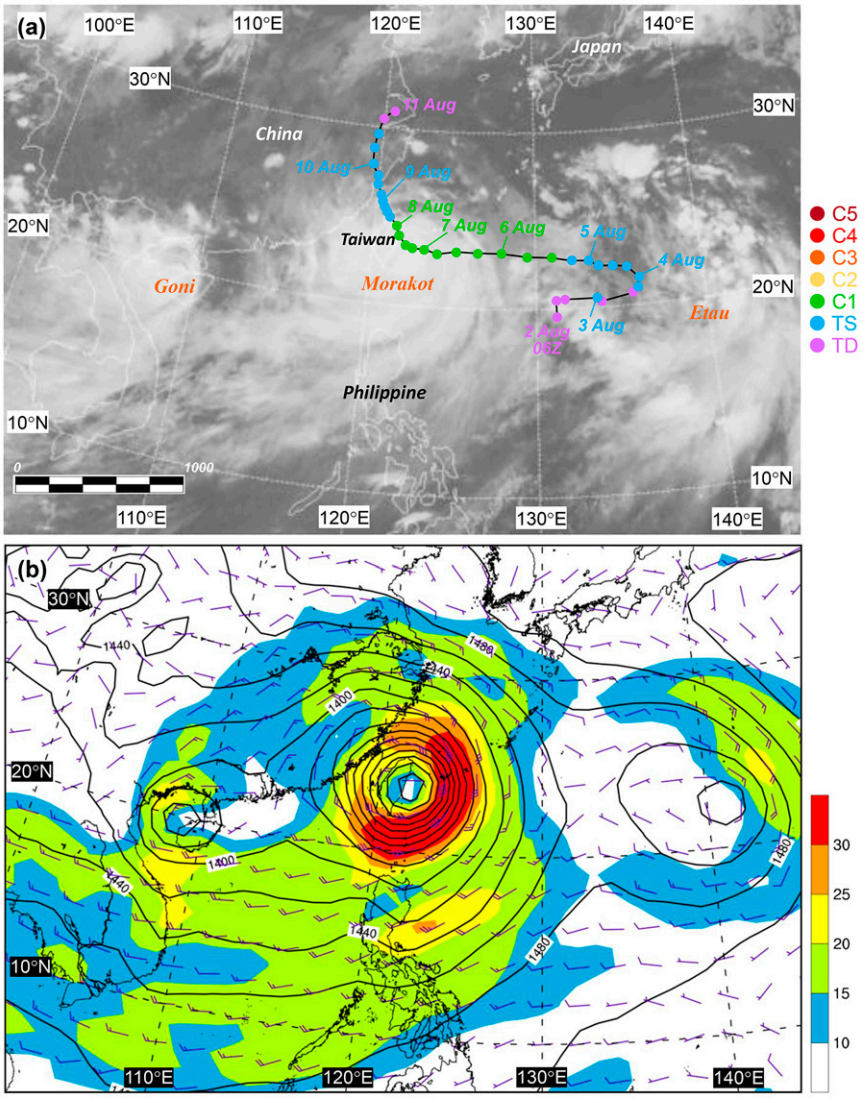

FIG. 2. (a) The CWB best track of TY Morakot (2009) overlaid with MTSAT IR cloud imagery at 1200 UTC 7 Aug 2009. The TC positions are given every 6 h (labeled at 0000 UTC), with intensity based on 10-min-averaged wind speed at 10-m height (on the Saffir–Simpson scale) shown in color. (b) The NCEP FNL analysis of geopotential height (gpm; contours) and horizontal winds [m s^{-1}; full (half) barb = 10 (5) m s^{-1}, wind speed shaded] at 850 hPa at 1200 UTC 7 Aug 2009.

its track change and slow motion near Taiwan were closely linked to the evolution of a monsoon gyre (Lander 1994) that was 4000 km in size at the intraseasonal time scale and included two other TCs (Goni and Etau) besides Morakot (Fig. 2). While Morakot never reached category 2 on the Saffir–Simpson scale, it moved very slowly as it impacted Taiwan during 7–9 August, and thus produced peak rainfalls of 1663 mm in 24 h, 2635 mm in 48 h, and 2748 mm in 72 h (Hsu et al. 2010; Wang et al. 2015). The 48-h total exceeds the world record of 2493 mm (Burt 2014; World Meteorological Organization World Archive of Weather and Climate Extremes: http://wmo.asu.edu/#global).

In one of the earliest studies on Morakot, Hong et al. (2010) applied wavelet analysis and demonstrated that the cyclonic gyre at submonthly time scales propagated from southeast to northwest toward Taiwan at about 5 m s^{-1} during early August 2009 (Figs. 3a–c), which led to Morakot being embedded in an easterly steering flow after formation. As the gyre continued to propagate northwestward, its center became collocated with Morakot (at synoptic scale) around 8 August (cf. Fig. 3a and Fig. 2a), which led to a weak steering flow for the storm. However, the gyre contributed to a strong surge in westerly to southwesterly flow toward southern Taiwan during and following 7 August. The moisture-laden southwesterlies impinging on southern Taiwan were most evident on 8 August (Fig. 3c), and was superposed and enhanced by waves at time scales beyond one month (Fig. 3d, also Chen and Shih 2012; J.-M. Chen et al. 2013). This surge of southwesterly flow led to the northward turn of Morakot.

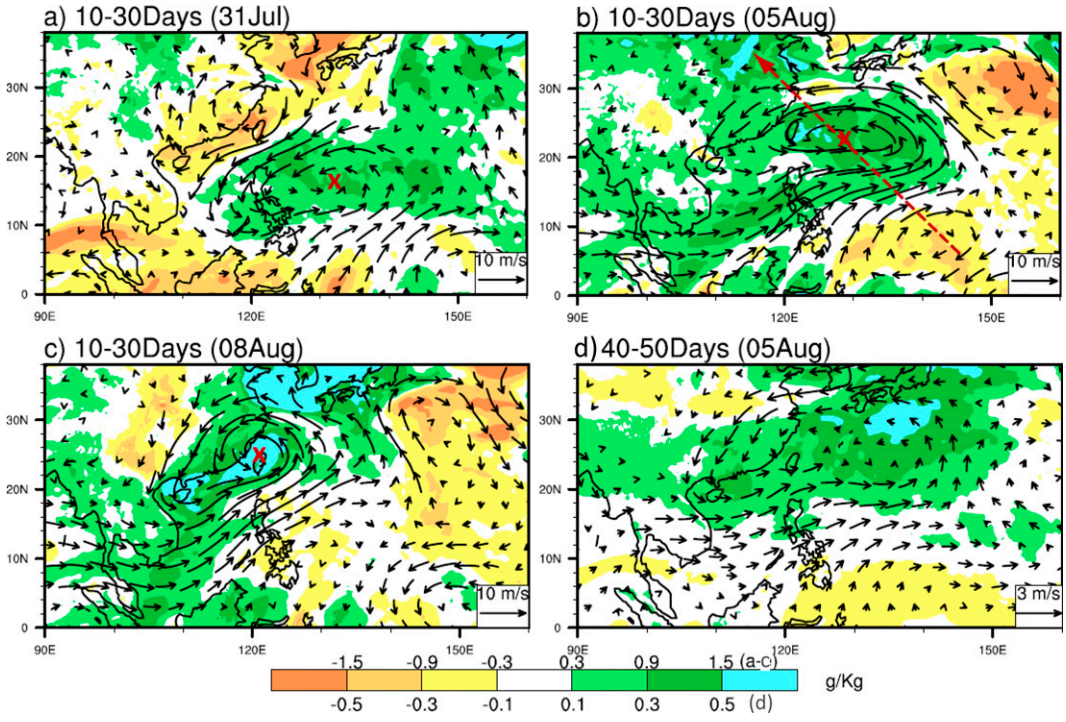

FIG. 3. (a)–(c) ECMWF-YOTC (0.25° × 0.25°) 10–30-day time-filtered wind and moisture anomalies at 850 hPa (top labels on the color scale), centered on (a) 31 Jul, (b) 5 Aug, and (c) 8 Aug 2009, respectively. The center of the submonthly circulation is marked by a red "X," and the red dashed arrow in (b) indicates its propagation direction. (d) As in (b), but for the 40–50-day perturbation on 5 Aug 2009 (bottom labels on the color scale). All panels are adapted from Fig. 3 of Hong et al. (2010).

In Wu et al. (2011) and Liang et al. (2011), Morakot was also found to be influenced by intraseasonal oscillations: its northward turn near Taiwan was likely caused by the TC interacting with a gyre at the quasi-biweekly (QBW) time scale (10–20 days) in the lower troposphere, similar to as depicted in Figs. 3a–c. Using numerical experiments, Liang et al. (2011) showed that without the QBW flow, a sharp northward turn similar to what occurred in the observations and in a control (CTL) experiment does not occur. Nor does the westward movement occur prior to landfall without the synoptic-scale (<10 day) flow (Fig. 4a, also Huang et al. 2017). Additional sensitivity tests in which the topography of Taiwan was reduced and removed confirmed that the topography had only a minor effect on the track (Fig. 4b, Liang et al. 2011). Therefore, the track of Morakot was mainly influenced by the background steering flow. Wu et al. (2013) found that such interactions of synoptic disturbances with the background gyre, including a gyre with a time scale > 20 days such as the Madden–Julian oscillation (MJO) in some cases, can account for the sudden track change of many TCs in the WNP (see also Liang and Wu 2015; Huang et al. 2017). Among other factors, trough interactions during extratropical transition can also cause changes in TC tracks (e.g., Archambault et al. 2013; Evans et al. 2017), but they tend to occur near midlatitudes under a faster moving speed, so are less relevant to Morakot. The slow translation of TY Morakot (2009) as it passed over Taiwan (cf. Fig. 2a), over a duration estimated to be 64 h by Chien and Kuo (2011), has been identified by many studies as a key factor contributing to the extreme rainfall of Morakot, if not the most important factor (also Yen et al. 2011; Wang et al. 2012).

Linked to the evolution of the background monsoon gyre and the overall slow motion of TY Morakot (2009) near Taiwan, the southwesterly flow surge (cf. Fig. 3c; Hong et al. 2010; J.-M. Chen et al. 2013) counteracted the initial easterly background flow and thereby led to the northward turn. In addition, the southwesterly surge enhanced the low-level moisture supply (≥16 g kg^{-1} over 950–700 hPa; C.-Y. Lin et al. 2011) to such an extent that it surpassed all other TCs with a similar track since at least 1977 (Chien and Kuo 2011; also Ge et al. 2010; Nguyen and Chen 2011; Yu and Cheng 2013; Huang and Chao 2013; Y.-H. Chen et al. 2017). As Morakot was impacting Taiwan, the strong southwesterly flow converged with the northwesterly flow around the TC at low levels over the southern Taiwan Strait to form a primary rainband that was highly asymmetric with deep convection especially to the south of the TC center, as shown in Fig. 5 and many observational studies (e.g., Chen et al. 2010; Jou et al. 2010; Wei et al. 2012). While this persistent, asymmetric rainfall pattern was also consistent with the northerly vertical wind shear (VWS) of about 5 m s^{-1} (Corbosiero and Molinari 2002; Chien and Kuo 2011; Wang et al. 2012), the inner core of Morakot was weak and the rainbands were largely collocated

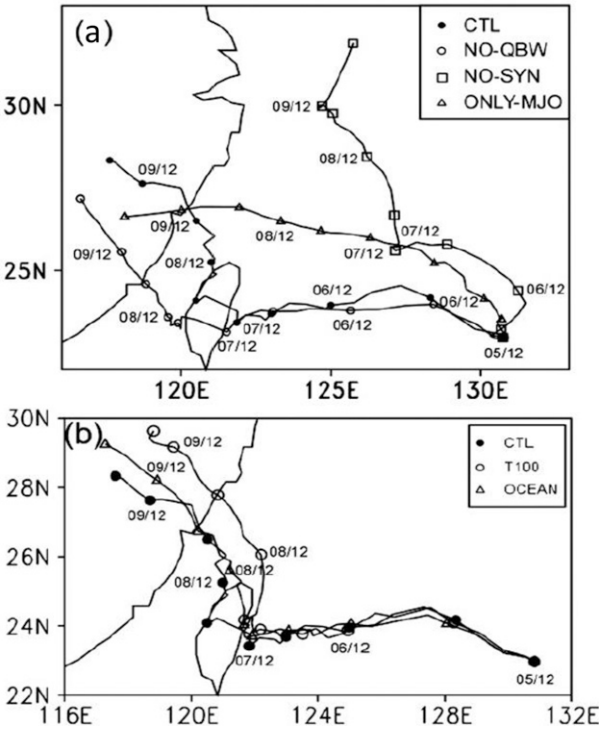

FIG. 4. Simulated tracks of TY Morakot with marks every 12 h from 1200 UTC 5 Aug to 0000 UTC 10 Aug 2009 in six sensitivity experiments: (a) CTL (control), NO-QBW (no QBW-scale flows), NO-SYN (no synoptic-scale flows), and ONLY-MJO (no QBW- or synoptic-scale flows, i.e., only MJO-scale flows) in initial fields, and (b) CTL, T100 (terrain of Taiwan limited to 100 m), and OCEAN (Taiwan replaced by ocean), respectively. All other settings in sensitivity test experiments are identical to the CTL (adapted from Figs. 8b and 10b of Liang et al. 2011).

with the outer circulation far from the center (Fig. 5, also Chen et al. 2010; Hall et al. 2013). This atypical structure was likely also linked to the low-frequency background gyre (Hong et al. 2010; Wu et al. 2011), which enhanced the southwesterly flow and its associated moisture supply (Chien and Kuo 2011; Nguyen and Chen 2011). During 8–9 August when Morakot was slowly moving away from Taiwan, the rainbands also expanded outward in conjunction with the topographic effect (Wu et al. 2011). In addition to the east–west-oriented (E–W) rainbands roughly parallel to the low-level flow, a north–south topographically forced rainband also formed and persisted along the windward (western) slopes of the CMR (cf. Figs. 1a and 5, also Liou et al. 2013). The terrain effect of Taiwan will be further discussed later.

Being unstable and rich in moisture, the southwesterly (to westerly) flow impinged on the CMR for a long period of time during Morakot, and its low-level (0.5–3 km) wind speed was nearly proportional to the areal-mean rain rate in the southern CMR, with a correlation coefficient R of 0.88 (Jou et al. 2010; Feng et al. 2012). This relationship can be explained by Huang et al. (2014), who found that the precipitation efficiency in this event was ~95% and almost all of the water vapor in uplifted air condensed and fell as precipitation. This precipitation efficiency value was also significantly higher than the values of ~60%–75% over the upstream ocean (Huang et al. 2014), and was presumably higher than in most other TCs near Taiwan. Thus, many studies (e.g., Chien and Kuo 2011; Huang et al. 2011; C.-Y. Lin et al. 2011; Xie and Zhang 2012) consider the concurrent large-scale surge in low-level southwesterly flow and its convergence with the circulation of TY Morakot (2009) as crucial to explaining the extreme rainfall of Morakot.

One of the most intriguing phenomena that stemmed from the case of Morakot is perhaps the effect and feedback of asymmetric latent heating (LH) on TC motion. Even though the large-scale deep-layer steering flow weakened as Morakot (2009) passed over Taiwan, gridded analyses indicate that the southerly steering flow remained around 10 km h^{-1} on 8 August (Chien and Kuo 2011; Wang et al. 2012). However, Morakot moved at only about 5–7 km h^{-1} and nearly stalled upon exiting Taiwan during this 24-h period (Fig. 2a), which is when the rainfall in the southern CMR was also the heaviest (Figs. 1a and 5; Wang et al. 2012). As mentioned, the rainbands and deep convection associated with TY Morakot (2009) were highly asymmetric and were concentrated in the southern quadrants of the storm during 8 August. Enhanced by the steep topography of Taiwan, such an asymmetric rainfall and LH were first hypothesized by Wang et al. (2012) to be the cause of the further slowdown of Morakot on 8 August 2009 (Fig. 5b), and thus were key factors that led to the extreme rainfall in southern Taiwan. In sensitivity tests in which the moisture content (and thus the LH effect) was reduced using the Cloud-Resolving Storm Simulator (CReSS), Wang et al. (2012, their Fig. 15) demonstrated that the stronger the asymmetric LH, the slower the TC moved away from Taiwan during 0000–1200 UTC 8 August. More recently, Y.-H. Chen et al. (2017) computed (azimuthal) wavenumber-1 (WN-1) potential vorticity (PV) tendency in a TC-relative, quasi-Lagrangian framework (Wu and Wang 2000) from a similar set of model sensitivity experiments, and confirmed that the LH (or diabatic heating) effect, with a large southeastward motion vector through PV generation, contributed to the slowdown of the departing Morakot on 8 August (Fig. 6, also Huang et al. 2017). Furthermore, it was mainly the E–W rainband that was collocated with a strong PV gradient (Fig. 6a), rather than the north-south rainband on the windward slope, that contributed to PV generation to the rear of the storm that caused the additional slowdown (Y.-H. Chen et al. 2017). Based on Chen et al. (2010) and Wang et al. (2012), this E–W rainband lasted for about 36 h (1200 UTC 7 August–0000 UTC 9 August) near southern Taiwan. Thus, the interaction among the environmental flow, TC track, its convection (if asymmetric), and the topography can prolong the rainfall impact period under certain circumstances in Taiwan. Recently, a similar interaction has also been shown to alter the structure of TS Kong-Rey (2013) by Wang et al. (2021).

While the tracks of many TCs in the past were likely affected by this asymmetric LH effect when they moved across Taiwan, this phenomenon was first described after TY Morakot (Wang et al. 2012, 2013a; Y.-H. Chen et al. 2017). Hsu et al. (2013)

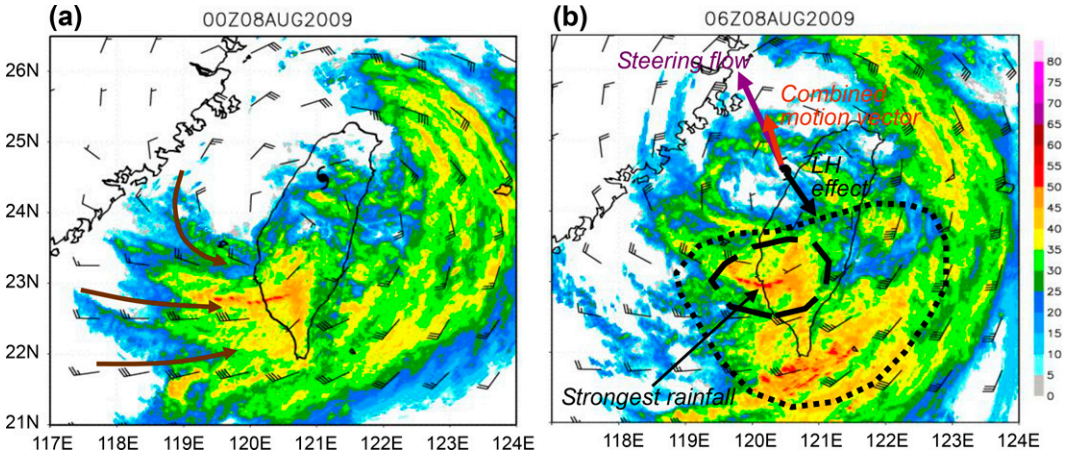

FIG. 5. Radar reflectivity vertical maximum indicator (VMI) composite (dBZ, scale on the right) near Taiwan, overlaid with the ECMWF-YOTC 850-hPa horizontal winds [m s^{-1}; full (half) barb = 10 (5) m s^{-1}] at (a) 0000 and (b) 0600 UTC 8 Aug 2009. The TC center is marked by the typhoon symbol. The general flow direction is depicted by the brown arrow lines in (a), and a schematic of the hypothesis of Wang et al. (2012) is shown in (b).

examined the translation speeds of 61 typhoons that made landfall on Taiwan from the east during 1960–2010, and the updated results through 2015 from 67 TCs are shown in Fig. 7 (from Su et al. 2017). For all TCs making landfall, their translation speeds tended to accelerate before landfall and then decelerate during the overland period and after departure (Fig. 7), which the authors attributed to the convection (and PV generation) phase-locked to Taiwan's topography. If the LH is intense and persistent enough, the topography can act to "attract" TCs and lengthen landfall duration. Hence, for slow movers with heavy rainfall such as Morakot, the slowdown is more significant, which suggests a positive feedback between typhoon rainfall in southern Taiwan and duration (red and blue curves, Fig. 7).

For the departure period of landfalling TCs, Y.-H. Chen et al. (2017) demonstrated that the total rainfall in Taiwan was highly correlated to the product of low-level southwesterly moisture flux upstream in the northern SCS and typhoon impact duration. This high correlation is especially relevant for TCs making landfall at 23°–24.5°N in the middle section of Taiwan (including Morakot), with an R as high as 0.93 (their Fig. 2b). The increased number of TCs with this type of track

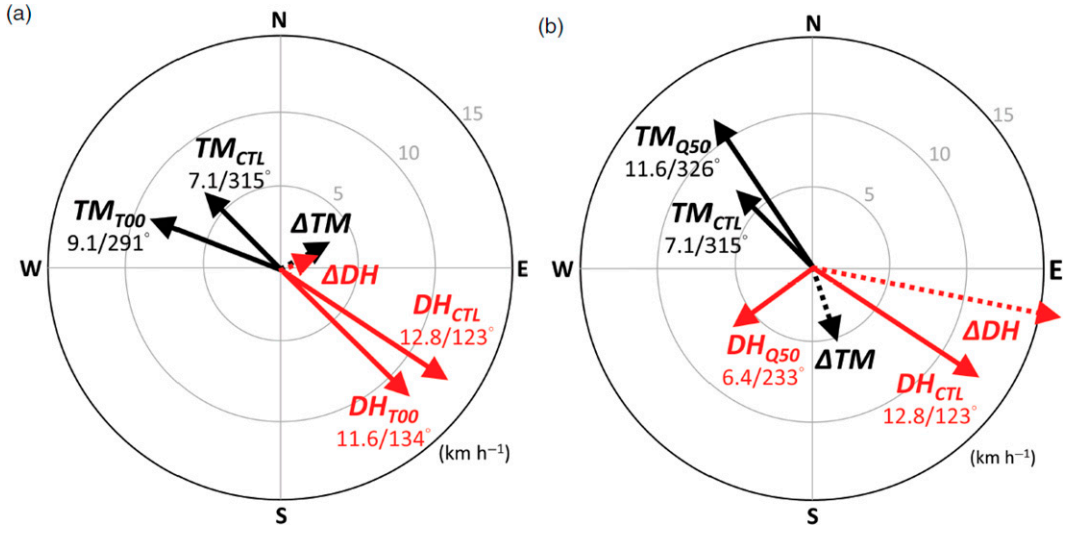

FIG. 6. WN-1 PV tendency diagnostic results of typhoon motion (TM, black) and diabatic heating (DH) terms averaged over 0000–1200 UTC 8 Aug from (a) CTL and T00 experiment in which the topography of Taiwan is flattened (but the E–W rainband remains) and (b) CTL and Q50 experiment in which the moisture content is reduced by 50% (but the north–south rainband remains). The TC center is at the origin. The translation speed (km h^{-1}) and direction (degree) are labeled, and ΔTM and ΔDH denote the vector differences (dash arrows, CTL minus the sensitivity test) (adapted from Fig. 7 of Y.-H. Chen et al. 2017).

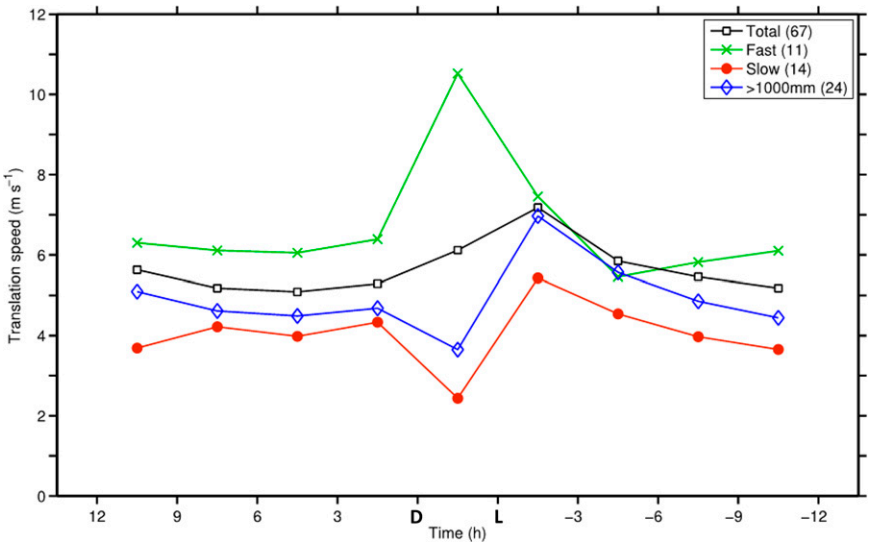

FIG. 7. Mean translation speeds (m s^{-1}; black curve) at 3-h intervals from 12 h before landfall ("L") to 12 h after departure ("D") for 67 westward-moving TCs during 1960–2015 that made landfall on the eastern coast of Taiwan and had a continuous track. The fast (green) and slow TCs (red) are subgroups that had overland translation speeds above and below one standard deviation, respectively. The rainy cases (blue) are those having CWB gauge rainfall amounts over 1000 mm (summed over 21 manned stations) while over land. The number of cases is given in the parentheses (adapted from Fig. 7 of Su et al. 2017).

(making landfall in central Taiwan) since 1988 compared to 1960–1988 (from 2 to 15), in combination with a long-term strengthening of the southwesterly flow (Y.-H. Chen et al. 2017), helps to explain the significant increase in TC rainfall in recent decades over Taiwan (Su et al. 2012; Chang et al. 2013).

Because TY Morakot (2009) was moving slowly and had a large size with a strong outer circulation about 150–300 km from its center (Fig. 5), southern Taiwan was under the impact of Morakot during most of 8–9 August (also Wu et al. 2011). To examine how the rainfall in Taiwan would differ if Morakot was smaller and had a weaker circulation, Wang et al. (2020) applied the piecewise PV inversion technique (PVIT; Davis and Emanuel 1991; Davis 1992) to produce a smaller/weaker TC vortex in the initial field at 0000 UTC 7 August 2009. For cases in which the inner-core PV was significantly reduced, the moist southwesterly flow was able to form the convergence zone with the TC circulation at smaller radii and impinge on Taiwan's topography earlier. With an increased LH effect in the inner core, the model TC vortex tended to spin up (e.g., Smith et al. 2009), make landfall earlier and exit later, and thus stay over Taiwan longer. Thus, this model result was in agreement with vortex kinematics and previous studies on asymmetric LH (e.g., Wang et al. 2012; Hsu et al. 2013; Y.-H. Chen et al. 2017). The rainfall in Taiwan was at least comparable to that in the control experiment in which the TC was not modified. However, the rain increased at smaller radii (roughly <250 km) in northern and central Taiwan, and decreased at larger radii (≥250 km) by up to 40% over the mountains in southern Taiwan. Thus, affected by its background gyre, the vortex structure of TY Morakot did appear to considerably influence the total rainfall in southern CMR.

The steep and complex topography of Taiwan has long been recognized to enhance rainfall amounts through forced uplift at the windward slopes and thereby dictate the overall TC-related rainfall distribution (Chang et al. 1993; Lin et al. 2001; Cheung et al. 2008; Yu and Cheng 2014) and for the monsoon flows (Kuo and Chen 1990; Chi 2006). The terrain-enhanced rainfall in Morakot included the moisture-laden southwesterly monsoon flow impinging on the southern CMR (cf. Fig. 1; Chien and Kuo 2011; C.-Y. Lin et al. 2011; Liou et al. 2013; Yu and Cheng 2013; Huang and Lin 2014). The contribution of Taiwan's topography to total Morakot rainfall has been assessed by several numerical sensitivity tests with estimates as high as 50%–80% of the peak amounts (Ge et al. 2010; Fang et al. 2011; Huang et al. 2011; Wang et al. 2012; Xie and Zhang 2012; Huang et al. 2014). Yu and Cheng (2014) used Doppler radar observations and estimated that about 57% of the total rainfall in Morakot was due to the orographic enhancement by the southern CMR. Although there are differences in the estimates, Yu and Cheng (2013) argue that the topography of Taiwan is the most influential factor on the amount of rain produced by Morakot. However, note that the role of the topography is similar to all TC rainfall in Taiwan and not unique to Morakot (e.g., Wu and Kuo 1999).

During the Morakot event, TS Goni was over the northern SCS (cf. Fig. 2). In the WNP, binary TC interactions (e.g., Fujiwhara 1921; Kuo et al. 2000; Wu et al. 2003; Hoover and Morgan 2011; Jang and Chun 2015) are not uncommon. Huang et al. (2011) and Huang and Chao (2013) investigated whether Goni might play a role in strengthening and channeling the southwesterly flow toward southern Taiwan. Using data assimilation in the four-dimensional variational

(4DVAR) analysis system (Zou et al. 1997; Zou and Xiao 2000) of the fifth-generation Pennsylvania State University–National Center for Atmospheric Research (PSU-NCAR) mesoscale model (MM5; Dudhia et al. 2005), the vortex of Goni was removed from the initial field at 0000 UTC 6 August. Without Goni, the model-simulated maximum 72-h rainfall (6–8 August) in southern Taiwan is reduced by about 25% (from 2323 to 1737 mm) compared to the CTL experiment (Huang et al. 2011), in general agreement with the assessment by Nguyen and Chen (2011). Xu and Lu (2014) had a similar estimate with a roughly 1/3 reduction in the peak rainfall amount. Among other factors influencing Morakot, I.-I. Lin et al. (2011) examined the effect of a warm ocean eddy that Morakot encountered (on 6 August) before making landfall in Taiwan. They found that the eddy increased the air–sea enthalpy flux supply by ~200% and contributed to about 10% of the rainfall. In general, warm ocean eddies affect TCs more in intensity than rainfall (e.g., Lin et al. 2009; Kuo et al. 2018).

The persistent and quasi-stationary E–W rainband over the Taiwan Strait contributed to the total rainfall in the plains over southwestern Taiwan (Wang et al. 2015), and such a scenario can also impact coastal regions severely under suitable conditions, such as in the case of Hurricane Harvey in 2017 (e.g., Fernández-Cabán et al. 2019; Zhang et al. 2019). Inside this rainband associated with Morakot, vigorous convective cells were observed to repeatedly form, evolve, and propagate, with frequent cell merging, strengthening, and back-building behavior (e.g., Doswell et al. 1996; Johnson and Mapes 2001; Chen et al. 2010; Wei et al. 2014). After moving onshore, these cells produced heavy rainfall and led to widespread flooding over the southwestern plains of Taiwan (C.-Y. Lin et al. 2011; Wang et al. 2015).

Wang et al. (2015) studied the convective-scale processes and interaction between the updrafts of convective cells inside this rainband and the background VWS. This VWS was associated with a westerly low-level jet (LLJ) of about 45 m s^{-1} near 1 km in height (also Wei et al. 2012), and thus had a hairpin shape in the hodograph. Below the LLJ, the interaction would produce negative (positive) dynamic pressure perturbations (p'_d) ahead and east (behind and west) of convective updrafts, as is typically found in midlatitudes (Rotunno and Klemp 1982; Klemp 1987). Above 1 km, the easterly VWS would produce positive (negative) p'_d perturbations east (west) of the convective updrafts. As depicted in Fig. 8, this vertical coupling of p'_d patterns would generate an upward-directed perturbation pressure gradient force that would lead to an enhancement of updrafts to the rear (west) side, which would tend to slowdown the propagation of mature cells. Such a slowing of the propagation would promote merging with new cells, low-level convergence, and convective back-building (Wang et al. 2015). These convective-scale processes also tend to enhance convective activity inside the rainbands and thus rainfall accumulation.

With much interest being given to the possible effects of anthropogenic climate change on extreme weather events (e.g., Knutson et al. 2010; Lackmann 2015), such a potential influence on the Morakot rainfall was accessed by Wang et al. (2019). Their CTL (Experiment E3A in Fig. 9a) was compared with a sensitivity test, in which they removed a long-term anthropogenic signal that was estimated as the mean difference between the historical and the all-natural runs of 18 Coupled Model Intercomparison Project Phase 5 (Taylor et al. 2012) models for 1985–2005. This sensitivity test indicates that Morakot in the modern climate might have yielded 3%–4% more rain inside a radius of 300–500 km from the storm center than its counterpart without the anthropogenic change. Therefore, the anthropogenic effect is not negligible, but a minor factor compared to those other factors reviewed above. This result is consistent with the study by Chang et al. (2013).

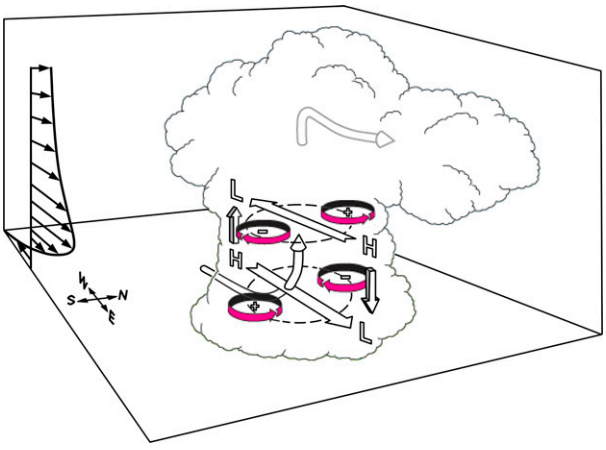

FIG. 8. Schematic of the distribution of dynamical pressure perturbations [indicated by "H" ("L") for an anomalous high (low)] inside a mature convective storm cell in an environment with westerly (easterly) vertical wind shear below (above) a westerly low-level jet (LLJ). In the case of the east–west rainband associated with Morakot, this configuration would favor slowdown of the propagation speed of mature cells and favor new development on the back side (adapted from Fig. 6 of Wang et al. 2015).

Finally, the extreme rainfall from Morakot also represents a unique opportunity to evaluate the accuracy of quantitative precipitation estimates from different remote sensing platforms. For example, S. Chen et al. (2013) suggest that all such products at various spatial resolutions underestimate the extreme rainfall of the event without additional correction from in situ rain gauge measurements. The underestimation is relatively small for ground-based radars (−18%) and the Tropical Rainfall Measuring Mission Multisatellite Precipitation Analysis 3B42RT (−19%). However, underestimates from some other satellite products are as much as from −30% to −60% compared to rain gauge data (S. Chen et al. 2013; also Hong et al. 2010; Liu et al. 2012; Zhou et al. 2015). Several methods have been proposed to improve rainfall estimates from radars using dual-polarimetric parameters (Liou et al. 2013) and statistical techniques (Kuo et al. 2014), or from satellite retrievals using analog to climatology (Liu et al. 2010), extrapolation (Ebert et al. 2011), and classification of orographic and nonorographic rainfall (Taniguchi et al. 2013).

From the above review, it is clear that several favorable and important factors were present simultaneously and interacted

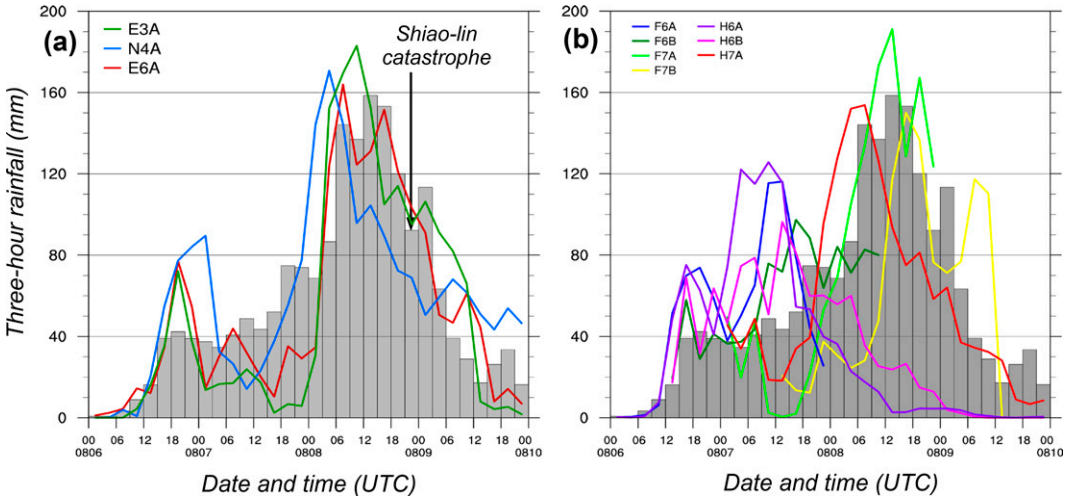

FIG. 9. (a) Histogram of observed (bars) and simulated 3-h rainfall (curves, all in mm) in three experiments by the CReSS model (taken from Wang et al. 2012, 2019), averaged inside the box shown in Fig. 1b (22.8°–23.65°N, 120.6°–120.95°E), over the 96 h during 6–9 Aug 2009. The first letter "E" ("N") in the experiment names denotes EC-YOTC (NCEP FNL) analyses used as IC/BCs, the middle number indicates the date of, and the final letter "A" represents 0000 UTC for the initial time. (b) As in (a), but for forecast and hindcast ("F" or "H" for the first letter in names) results (from Wang et al. 2013b). The final letter "B" represents 1200 UTC for the initial time. The time of the Shiao-lin catastrophe is marked in (a).

across the scales in synergy during TY Morakot (2009) to cause the extreme rainfall in Taiwan. These factors and their main interactions are summarized below and in Table 1, from large to small scale but adjusted by their importance. First, as Morakot moved across Taiwan, its background steering flow weakened and shifted from easterly to southerly, when the center of the monsoon gyre (intraseasonal time scale) became collocated with Morakot (synoptic scale), leading to the TC's slow translation speed and long impact duration. Second, a surge of low-level southwesterly flow, which was enhanced by the southern part of the monsoon gyre, supplied abundant moisture toward southern Taiwan and converged with TC circulation. Third, asymmetric LH effect (at mesoscale) in primary rainband (associated with the low-level convergence) south of storm center led to a further slowdown of Morakot's motion during its departure on 8 August, when the rainfall in southern Taiwan was the heaviest. Fourth, the steep mesoscale topography of Taiwan was estimated to at least double the peak rainfall amount from Morakot. Fifth, the large size of Morakot with strong outer circulation could have contributed to an increased rainfall in the southern CMR region. Sixth, the existence of TS Goni to the west of Morakot played a role in strengthening and channeling the southwesterly flow toward southern Taiwan. Seventh, the mesoscale warm ocean eddy, over which Morakot passed on 6 August, also contributed to the overall rainfall via increased enthalpy flux. Finally, the frequent back-building and

TABLE 1. A summary of major factors and their cause and/or main effect (with major references) as reviewed in section 2.

Factor	Cause and/or main effect
Weak steering flow and slow TC translation speed	Collocation of background monsoon gyre on the intraseasonal time scale with Morakot (Hong et al. 2010; Liang et al. 2011)
Strong surge of low-level southwesterly flow	Enhanced by the monsoon gyre and supplied abundant moisture toward southern Taiwan to converge with TC circulation (Chien and Kuo 2011)
Asymmetric LH effect south of Morakot's center	Caused further slowdown of Morakot during its departure on 8 Aug, when the rainfall in southern Taiwan was the heaviest (Wang et al. 2012; Y.-H. Chen et al. 2017)
Topography of Taiwan	Estimated to at least double the peak rainfall amount from the storm (Ge et al. 2010; Fang et al. 2011; Yu and Cheng 2014)
Large size of Morakot with strong outer circulation	Structural characteristics linked to background gyre and lengthened the heavy-rainfall period in southern Taiwan (Wu et al. 2011; Wang et al. 2020)
Existence of TS Goni	Strengthened and channeled the southwesterly flow toward southern Taiwan (Huang et al. 2011)
Warm ocean eddy before landfall	Contributed to rainfall through increased enthalpy flux (I.-I. Lin et al. 2011)
Back-building and cell merger inside the E–W rainband of Morakot	Due to interaction between convective updrafts and the westerly LLJ in the rainband environment, and led to rainfall increase in southwestern Taiwan (Wang et al. 2015)

merging behavior of convective cells inside the quasi-stationary E–W rainband over the southern Taiwan Strait at the storm scale, from the interaction between convective updrafts and the westerly LLJ in the environment, also led to enhancement of cells and thus rainfall in southwestern Taiwan. The first four factors are particularly important, as the extreme rainfall on 8 August during the departure stage of Morakot was a result of strong positive feedback and interaction among a weak steering flow (for longer duration), strong low-level southwesterly flow (for moisture supply), asymmetric rainfall and LH (for further slowdown), and the topography of Taiwan (for rainfall/LH enhancement).

3. Numerical simulations and forecast studies of TY Morakot (2009)

In this section, the modeling and forecast studies of Morakot are reviewed, including those that investigate the impact of different physical schemes or observational datasets in the data assimilation (DA) system. First, to answer the question whether the present-day models are capable of simulating the Morakot event, the results from various studies are compared with the observations of the peak accumulated rainfall amounts. However, even though the rain gauge network in Taiwan is quite dense (about 450 sites, Fig. 1a), the sampling resolution over the mountain interior in southern CMR is much lower than is available from the evenly spaced model grids (e.g., ~2250 points over Taiwan at $\Delta x = 4$ km). Thus, the observed maximum rainfall measured by the rain gauge network likely represents a lower bound of the true value.

In Table 2, the model-simulated peak rainfall amounts from the control (CTL) or "full-physics" experiments of various studies are compared with the observation, along with the basic information on model used, its configuration, initial and boundary conditions (IC/BCs), initial time (t_0), and accumulation length. Here, only simulations using gridded analyses for both IC and BCs are included, so that the track of Morakot is reproduced reasonably well. Under such circumstances, it is evident that the majority of the models, including the Weather Research and Forecasting (WRF) Model (Skamarock et al. 2005) in rows 1–3, 7–13, and 18; CReSS (Tsuboki and Sakakibara 2002, 2007) in rows 14–17; and the Coupled Ocean–Atmosphere Mesoscale Prediction System (COAMPS)–TC (Hodur 1997; Chen et al. 2003) in row 4; are capable of producing a peak rainfall amount (column 8) comparable to, if not slightly over, the observed maximum (column 9). As examples, the observed rainfall histogram (every 3 h) averaged over the southern CMR box in Fig. 1b are shown with histograms from three simulations (Wang et al. 2012, 2019) in Fig. 9a, including one that starts as early as 0000 UTC 3 August (E3A). These simulations can all reproduce the Morakot rainfall event reasonably well.

Some models in Table 2 generate an amount well exceeding the observation (e.g., Fang and Kuo 2013; Huang et al. 2014; rows 1 and 7). However, whether they truly have an issue of overforecasting remains to be clarified, given the observation-model difference in sampling resolution as mentioned. The models that do not predict a peak rainfall amount comparable to the observed value (say, less than ~80%) tend to be more coarse in horizontal resolution and are not convective-permitting models (e.g., 9-km WRF of Liang et al. 2011 in row 10; 15-km MPAS of Huang et al. 2017 in row 6) or with a fine domain smaller in size (e.g., Ge et al. 2010 in row 3; Huang and Chao 2013 in row 5). Clearly, an adequate resolution is necessary to properly simulate the finer-scale processes identified to be important in Morakot, such as cloud microphysics, asymmetric latent heat release, orographic effects, and VWS-updraft interaction inside the rainbands. As Morakot was also a large storm, a larger fine domain size is also helpful to better capture the cross-scale interactions among the above factors and with their background features, such as the interactions with the monsoon gyre, southwesterly flow, and Goni. Thus, the present-day state-of-the-art regional models, when configured properly and provided with IC/BCs at a sufficient quality, can certainly simulate and capture the Morakot rainfall event in a realistic fashion.

Other modeling studies also conducted sensitivity tests to determine and quantify the influence of model configurations and various physical schemes on the rainfall of Morakot. Hendricks et al. (2016) concluded that the extreme rainfall of Morakot is reasonably predictable, although the choice of cloud microphysics can affect the quantitative precipitation forecast (QPF). However, the intensity and the track of Morakot are more sensitive to the cumulus parameterization scheme than cloud microphysics. Also, consistent with the discussion above, a successful simulation requires a convective-permitting grid size (also Hall et al. 2013), but a finer grid with $\Delta x = 1.67$ km offers little additional benefit. Ming and Zhang (2016) found that Morakot's intensity and structure were sensitive to the surface flux parameterization scheme, but its track was not so sensitive.

Similarly to Table 2, results on Morakot from forecast and hindcast studies in which the BCs are from global model real-time forecasts (and thus contain larger errors that limit forecast accuracy) are summarized in Table 3. Most model deterministic forecasts, including those made by the MM5 in row 3 and the Advanced Regional Prediction System (ARPS, Xue et al. 2000, 2001) in row 1, are capable of predicting realistic peak rainfall amount as well if the lead time is short enough (i.e., with a t_0 at or after 0000 UTC 6 August and forecast range $\leq$ 48 h). One exception is some runs in the Wu et al. (2010) study (their Figs. 16–18), but those runs are not included in Table 3. The other exception is the study of Hendricks et al. (2011), in which the 5-km TC-following mesh was small (925 km $\times$ 925 km) and the predicted translation speed was too slow before and too fast after landfall, and consequently the peak rainfall was only about half the observed value. The authors attributed this deficiency to a predicted premature dissipation of Goni, an inaccurate interaction between Morakot and the southwesterly monsoon, and the coarse grid spacing that was inadequate to resolve the topography. Indeed, given the large size of Morakot, the domain of Hendricks et al. (2011) was likely too small to fully capture the key processes involved. Later, Hendricks et al. (2016, cf. Table 2), with an enlarged (and fixed) 5-km domain and an improved track forecast, the COAMPS-TC model could more successfully simulate the Morakot event.

Some forecast and hindcast results with a t_0 between 0000 UTC 6 August and 1200 UTC 7 August from Wang et al. (2013b)

TABLE 2. Numerical simulation studies of TY Morakot (2009), including the model used, major specifications, and the comparison in peak rainfall (mm) between their CTL and the observation. For the grid size (column 3), those of parent grids are also given if $\Delta x \leq 5$ km. For the domain size of the finest mesh (column 4), L, S, and M denote those larger than ($x \times y$) 1500 × 1200 km^2, smaller than 1000 × 800 km^2, and in between. The length of rainfall accumulation period (column 7) is given in days if both end points are at 0000 UTC (or in hours otherwise), and an asterisk in the observed rainfall (column 9) denotes data from another (or this) study (for the same period). The source (column 10) refers to the figure or table. Abbreviations not yet defined in the text are as follows: DART: DA Research Testbed; EAKF: ensemble adjustment Kalman filter; NOGAPS: Navy Operational Global Atmospheric Prediction System; MM5: Mesoscale Model version 5; MPAS: Model for Prediction Across Scales; ERA: ECMWF Re-Analysis; TOGA: Tropical Ocean Global Atmosphere.

Paper	Model (version)	Grid size (Δx, km)	Fine domain size	IC/BCs (resolution)	Initial time (t_0)	Accumulation length (Δt)	Peak rainfall (mm)	Obs rainfall (mm)	Source
Fang and Kuo (2013)	WRF (3.1.1)	4	L	ECMWF (0.225°, 6 h) + WRF DART EAKF	0000 UTC 6 Aug	3 days	4885 2530	2410	F15
Fang et al. (2011)	WRF (3.1.1)	4	L	ECMWF (0.225°, 6 h) + random perturbations	0000 UTC 6 Aug	4 days	3128	2874	F1
Ge et al. (2010)	WRF	3	S	NCEP FNL (1°, 6 h)	1200 UTC 5 Aug	108 h	~1800	≥2874*	F2
Hendricks et al. (2016)	COAMPS-TC	1.67, 5	M	NOGAPS (1°, 6 h)	1200 UTC 6 Aug	72 h	2700	2645*	F9
Huang and Chao (2013)	MM5 (3.7)	5	S	NCEP FNL (1°, 6 h)	0000 UTC 6 Aug	1 day	1273	1663*	F5
Huang et al. (2017)	MPAS (4.0)	15	L	ERA Interim (0.5°, 6 h)	0000 UTC 6 Aug	3 days	~1900	2683*	F5
	WRF	15	L				~1750		
		5	S				~1900		
Huang et al. (2014)	WRF (3.2)	1, 3	S	ECMWF TOGA (1.125°, 6 h)	0000 UTC 6 Aug	3 days	~5000	2683	F4
						1 day	~2000	~1450	
Huang and Lin (2014)	WRF	3	S	NCEP FNL (1°, 6 h)	0000 UTC 3 Aug	120 h	3505	2851	F5
						24 h	1931	1402	F6
Lee et al. (2013)	WRF (3.2)	1.67, 5	S	NCEP FNL (1°, 6 h)	0000 UTC 4 Aug	100 h	~3500	2885	F8
						4 days	2780	2777	F9
Liang et al. (2011)	WRF	9	L	NCEP FNL (1°, 6 h)	1200 UTC 5 Aug	108 h	~1900	≥2874*	F6
		3	S			24 h	~1300	1036	F5
C.-Y. Lin et al. (2011)	WRF (3.1)	3	L	NCEP FNL (0.5°, 6 h)	0000 UTC 6 Aug	4 days	~3600	2855	F1, F6
Nguyen and Chen (2011)	WRF (3.1.1)	6	L	NCEP FNL (1°, 6 h)	0000 UTC 6 Aug	5 days	~2900	~3000*	F18
						3 days	~2500	2410*	F12
Tao et al. (2011)	WRF (3.1.1)	2	S	NCEP FNL (1°, 6 h)	0000 UTC 7 Aug	3 days	3171	2705	F3
Wang et al. (2012)	CReSS (2.3)	3	L	ECMWF YOTC (0.25°, 6 h)	0000 UTC 6 Aug	4 days	~3500	2855	F2, F12
						2 days	~2600	~2000	
Wang et al. (2013b)	CReSS (2.3)	3	L	ECMWF YOTC (0.25°, 6 h)	0000 UTC 6 Aug	1 day	~1650	1663*	F4
			L	NCEP FNL (1°, 6 h)	0000 UTC 4 Aug	4 days	~3300	2855	
						1 day	~1300	1663*	
Wang et al. (2019)	CReSS (2.3)	3	L	ECMWF YOTC (0.25°, 6 h)	0000 UTC 3 Aug	4 days	~3200	2855	F5
Wang et al. (2020)	CReSS (2.3)	2.5	L	ECMWF YOTC (0.25°, 6 h)	0000 UTC 7 Aug	3 days	~3200	2748	F8
Yen et al. (2011)	WRF (2.2.1)	3.33	S	NCEP FNL (1°, 6 h)	0000 UTC 6 Aug	36 h	1800	1609	T1, F6

TABLE 3. Forecast and hindcast studies of Morakot as in Table 2, but the BCs are from global model real-time forecasts. Additional information is given in column 7 on the starting time of the accumulation period (t_S) to indicate the verification range in forecasts. Abbreviations not given earlier (in the text and Table 2) are as follows: 3DVAR: three-dimensional variational analysis; GFS: Global Forecast System; and EDA: ensemble DA.

Paper	Model (version)	Grid size (Δx, km)	Fine domain size	IC/BCs (resolution)	Initial time (t_0)	Starting time of accumulation (t_S)	Accumulation length (Δt)	Peak rainfall (mm)	Obs rainfall (mm)	Source
Hall et al. (2013)	ARPS (5.2)	3	L	NCEP GFS (0.5°)	0000 UTC 7 Aug	1200 UTC 7 Aug	36 h	2174	2226	F14, F17
Hendricks et al. (2011)	COAMPS-TC	5	M	NOGAPS + COAMPS-TC 3DVAR	1200 UTC 6 Aug	1200 UTC 6 Aug 1200 UTC 6 Aug	72 h 48 h	1319 960	2645 2003	T1, F5
Huang et al. (2011)	MM5 (3.7)	5	S	NCEP GFS (1°)	0000 UTC 6 Aug	0000 UTC 6 Aug 0000 UTC 8 Aug	3 days 1 day	2323 1273	2403 1663*	F3, F7
Schwartz et al. (2012)	WRF	5	S	NCEP GFS + DA-EAKF	1200 UTC 6 Aug	1200 UTC 6 Aug	72 h	2246	2638	F6
Wang et al. (2013b)	CReSS (2.3)	3	L	NCEP GFS (1°, 3 h)	0000 UTC 6 Aug	0000 UTC 6 Aug	3 days	~2300	2410*	F13
	CReSS (2.2)	4	M		1200 UTC 6 Aug 0000 UTC 7 Aug	1200 UTC 6 Aug 0000 UTC 8 Aug	48 h 1 day	~1950 ~1800	~2000 1663*	F11
Wang et al. (2022)	CReSS (2.3)	2.5	L	NCEP GFS (0.5°, 3 h)	1200 UTC 6 Aug–0000 UTC 8 Aug, every 6 h	1200 UTC 7 Aug 0000 UTC 8 Aug	48 h 1 day	1427–3836 714–2366	2635 1663	F4 F9
Wu et al. (2010)	WRF (3.1.1)	5	S	NCEP GFS (1°) + WRF 3DVAR	0000 UTC 6 Aug–0600 UTC 10 Aug, every 6 h	1200 UTC 6 Aug–1800 UTC 10 Aug 1200 UTC 7 Aug–1800 UTC 11 Aug	108 h[a]	1978–3037 1803–2797	2882	F11 F13
Xie and Zhang (2012)	WRF	4.5	L	NCEP GFS EDA	0000 UTC 5 Aug	0000 UTC 6 Aug	3 days	1851–3545	2410	F4
Xie et al. (2013)	WRF (3.1.0)	4.5	L	NCEP GFS EDA	0000 UTC 5 Aug	0000 UTC 6 Aug	3 days	2762[b]	2410	F1
Zhang et al. (2010)	WRF	4.5	L	NCEP GFS EDA	0000 UTC 5 Aug	0000 UTC 6 Aug	3 days	3545 1274	2410	F1

[a] These plots were produced by summing and averaging the 12–24 h (or 36–48 h) QPFs by runs every 6 h initialized over the 4.5-day period indicated (with a total of 18 runs).
[b] From the deterministic forecast using the ensemble mean of the EDA as IC/BCs.

are also shown in Fig. 9b. Using NCEP GFS analysis and forecasts as IC/BCs, the peak rainfall occurred too early (during 1200 UTC 7 August–0000 UTC 8 August) in association with a track error being too fast when t_0 is on 6 August. In these forecasts, even though the areal-averaged 3-hourly peak rainfall in southern CMR can reach about 100–120 mm and ≥60% of the observed value (~160 mm per 3 h), the whole Morakot event would not last as long (Fig. 9b). In the shorter lead-time forecasts executed during 7 August, the errors in timing, duration, and (peak) magnitude of rainfall would all be reduced considerably. In F6A that produced the lowest peak rainfall amount in 48 h (among those shown), it nevertheless reached 2/3 of the observed value (Wang et al. 2013b). As shown in Table 3, most studies examined heavy rainfall accumulated over a period at least 24 h, which is relatively long. When the categorical statistics are used (e.g., Schaefer 1990; Wilks 1995) beyond the range of about 1.5 days, the issue of double penalty (e.g., Ebert and McBride 2000; Davis et al. 2006) would severely penalize the models that can predict the event magnitude, but too early (and/or too short). That is, the penalty would be not only in space but also in time (cf. Fig. 9b, also Fang et al. 2011), which is a situation not ideal (and potentially misleading) for model verification (e.g., Wang 2014). Due to the continuous improvement in global models and the quality of their analyses/forecasts, the lead time at which a good QPF can be produced for the majority of typhoons can be expected to be longer (i.e., in an earlier forecast) compared to that of Morakot (e.g., Wang et al. 2016).

There are also studies that discuss the various efforts to improve the initial conditions in TC environment through DA for TY Morakot (2009). Several types of observations and their impacts have been investigated, including microwave radiances from polar-orbiting satellites (Schwartz et al. 2012) and the *FengYun-3A* (*FY-3A*) satellite microwave data (Yang et al. 2013). The impact of assimilating dropwindsonde data that were obtained in the Dropwindsonde Observations for Typhoon Surveillance near the Taiwan Region (DOTSTAR) program (Wu et al. 2005) at 0000 UTC 6 August for Morakot in both the NCEP and the ECMWF's deterministic global models was also investigated by Chou et al. (2011). The authors found that TY Morakot was one of the worst cases because the dropsonde data had a negative impact on Morakot's track forecast mainly during the departure stage. This was in contrast to an average improvement of about 10%–20% for days 1–5 for all TCs studied, and the same dropsonde data ingested into the MM5 3DVAR system were found by B. Chen et al. (2013) to have some positive impact on simulated track of Morakot within 36 h. Qin and Mu (2011) also found similar improvements with MM5 simulations using NCEP reanalyses as first guess and BCs. In some sense, such different results also indicate the importance of model resolution for predicting the Morakot event.

Nguyen and Chen (2011) developed a dynamic initialization technique to spin-up the TC vortex by repeated model integrations for short periods (of ~30 min) while being relocated in the same time-invariant environment (at t_0) for a number of multiple cycles as needed. When applied to Morakot, this technique was shown to generate a realistic TC that had characteristics consistent with its background flow, such as the vortex wind asymmetry, and thus had certain advantages over methods such as bogus vortex assimilation (e.g., Huang et al. 2011). Because this dynamic initialization technique would require additional computer time for operational use, Nguyen and Chen (2014) subsequently revised the technique for better efficiency, by inserting an artificial warm core to accelerate the spinup process.

Because the uncertainty in Morakot's track forecasts was high at initial times prior to 0000 UTC 6 August 2009 (Yeh et al. 2010; Wang et al. 2013b), an ensemble approach was applied to assess its probability to strike Taiwan (e.g., Zhang et al. 2010; Hamill et al. 2011; Fang et al. 2011; Xie et al. 2013). In general, the accuracy of the NCEP GFS ensemble was lower than that of ECMWF ensemble for the Morakot event. These ensembles can benefit from a more advanced DA system such as the ensemble Kalman filter (EnKF) method, which Hamill et al. (2011) demonstrated would improve the steering flow. Zhang et al. (2010) found that about 20% of a 60-member ensemble initiated at t_0 = 0000 UTC 5 August produced a peak 3-day rainfall ≥ 2000 mm, with an overall ensemble mean of 1274 mm (their Fig. 1, cf. Table 3). At the range of 24–96 h, their ensemble results indicate a fair likelihood (≥30%–50%) for a large portion of Taiwan to receive ≥500 mm of rainfall (Fig. 10a), and more importantly, some chance (about 10%–40%) of extreme rainfall exceeding 1500 mm to occur in the southern CMR (Fig. 10b) for the period of 6–8 August. Thus, Zhang et al. (2010) demonstrated the potential benefit of ensemble-based analysis and forecasting using convective-permitting models (Δx = 4.5 km) for the Morakot event in real time, if sufficient computing resources are made available. For the Fang et al. (2011, cf. Table 2) 32-member WRF ensemble simulations from 0000 UTC 6 August, the mean and probabilities of extreme rainfall were raised considerably (Figs. 10c,d) compared to Zhang et al. (2010), although the lead time was shortened by 24 h and the peak rainfall timing tended to be slightly early. In addition, Fang and Kuo (2013) recommended a combined low- and high-resolution (4 km) lagged ensemble for improved efficiency in terms of computational resources.

Wang et al. (2022) recently also applied the time-lagged strategy to produce ensemble QPFs for the Morakot event using the CReSS model, with Δx = 2.5 km (Table 3) and a configuration identical to that of Wang et al. (2016). With one run out to eight days (192 h) every 6 h, the temporal evolution of heavy-rainfall probability could be examined. Wang et al. (2022) found that most of the members initialized at and after 0600 UTC 6 August when the track errors became sufficiently small, could capture the extreme rainfall of Morakot reasonably well, with a peak 48-h amount near or over 2500 mm. At longer lead times, the predictability was limited by larger track errors, and therefore a sharp increase existed in the derived heavy-rainfall probabilities starting from 6 August, as shown in Fig. 11. For model initialization times between 0000 UTC 6 August and 1200 UTC 7 August, ≥80%–90% of the runs indicated a 48-h rainfall (for the target period starting from 1200 UTC 7 August) over 1000 mm in the southern CMR of Taiwan (Fig. 11g), and ≥70% of them predicted in excess of 1500 mm in parts of the area (Fig. 11h). Note that even at

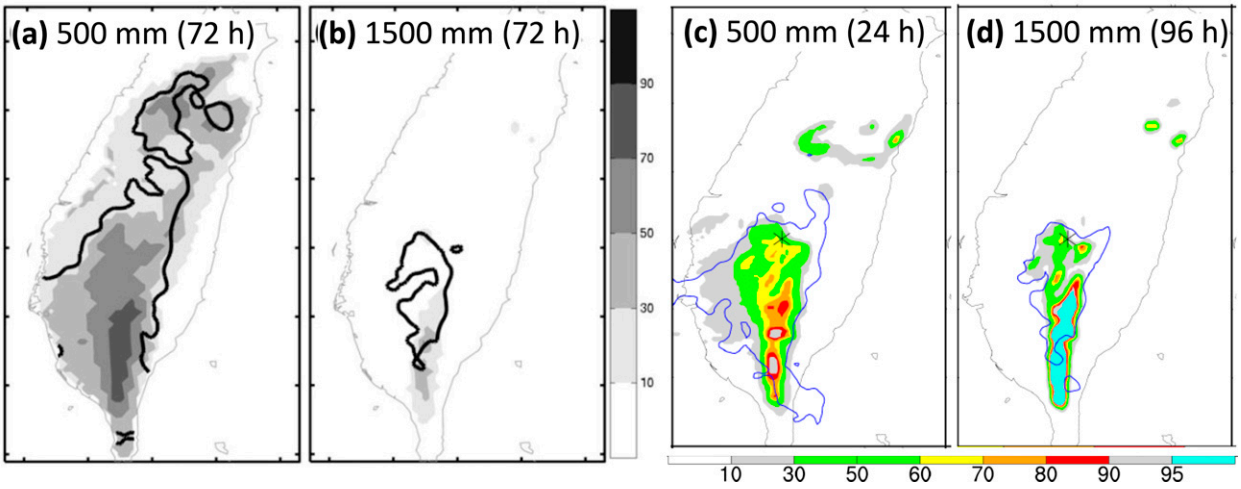

FIG. 10. Probability distribution (%) of the 72-h rainfall (for 6–8 Aug) exceeding threshold values of (a) 500 and (b) 1500 mm, estimated from the 60-member WRF ensemble initialized with EDA perturbations (t_0 = 0000 UTC 5 Aug). The observed rainfall areas reaching the specified thresholds are depicted by thick solid contours (adapted from Fig. 7 of Zhang et al. 2010). (c),(d) As in (a) and (b), but for 24-h rainfall (for 8 Aug) exceeding 500 mm in (c) and 96-h rainfall (for 6–9 Aug) exceeding 1500 mm in (d), estimated from the 32-member WRF ensemble simulation (t_0 = 0000 UTC 6 Aug). The observed rainfall areas are depicted by blue contours (adapted from Fig. 17 of Fang et al. 2011).

1200 UTC 7 August (i.e., t_0 of the last run used in Fig. 11), the Shiao-Lin catastrophe would still be more than 1.5 days away. Therefore, the time evolution of the probability from a lagged ensemble may provide timely and valuable information to the authorities for hazard preparation and mitigation. As the computational cost of Wang et al. (2022) is estimated to be only a fraction of those used in Zhang et al. (2010) and Fang et al. (2011), the cost-effectiveness of the time-lagged method also makes it a more feasible and affordable option at the present time, at least until ample computational resources become available, in agreement with Fang and Kuo (2013).

In conclusion, the extreme rainfall of TY Morakot (2009) is predictable with present-day models with an adequate resolution, at least at short range with a t_0 on 6 August or later, when the track errors are reasonably small for the complex interactions and feedbacks among the background, southwesterly flow, asymmetric rainfall, and topography of Taiwan in this case to take place in synergy. The above results are in agreement with Wang et al. (2013b, 2022), Fang and Kuo (2013), and Hendricks et al. (2016). While these studies were all targeted on Morakot (2009), many of the findings may be applicable to other WNP TCs.

4. Summary and conclusions

During 7–9 August 2009, TY Morakot struck Taiwan and brought record-breaking extreme rainfall to the southern part of the island, and especially over the interior of the CMR (Fig. 1). The maximum rainfall amount was 1663 mm in 24 h and 2635 mm in 48 h, and the latter rainfall exceeded the official world record. The death toll of nearly 700 was largely caused by a single massive mudslide, and thus Morakot became the deadliest TC in Taiwan since 1959. In this paper, past studies of this category-2 but devastating "perfect storm" in Taiwan are reviewed to examine key physical mechanisms to answer the question "What have we learned about TY Morakot (2009)" or "What was unique or special about this storm?"

Multiple favorable factors have been found to occur simultaneously and interacted in synergy to bring about the extreme rainfall of Morakot and its impacts in Taiwan. Among these factors, the most important ones are:

- Slow translation speed: TY Morakot (2009) moved very slowly across Taiwan and changed its course from westward to almost directly northward (Fig. 2). At the large scale, a preexisting monsoon gyre on the migrated northwestward to become collocated with Morakot, and the easterly steering flow weakened and gradually changed to southerly to contribute to the slow motion of Morakot near Taiwan (Figs. 3 and 4).
- Strong surge of low-level southwesterly flow: The southwesterly flow constituted the southern part of the monsoon gyre (Fig. 3) and supplied a strong moisture flux toward southern Taiwan that converged with the northerly TC flow to lead to a persistent and asymmetric rainfall pattern near southern Taiwan (Fig. 5).
- Asymmetric rainfall pattern and LH effect: The LH effect near southern Taiwan caused Morakot to further slowdown as it began moving away from the island on 8 August, when the rainfall in the southern CMR was the heaviest (Figs. 5, 6, and 9).
- Steep topography: The topography of Taiwan was estimated to at least double Morakot's peak rainfall amount compared to flat terrain. However, this is not a unique factor only in Morakot.

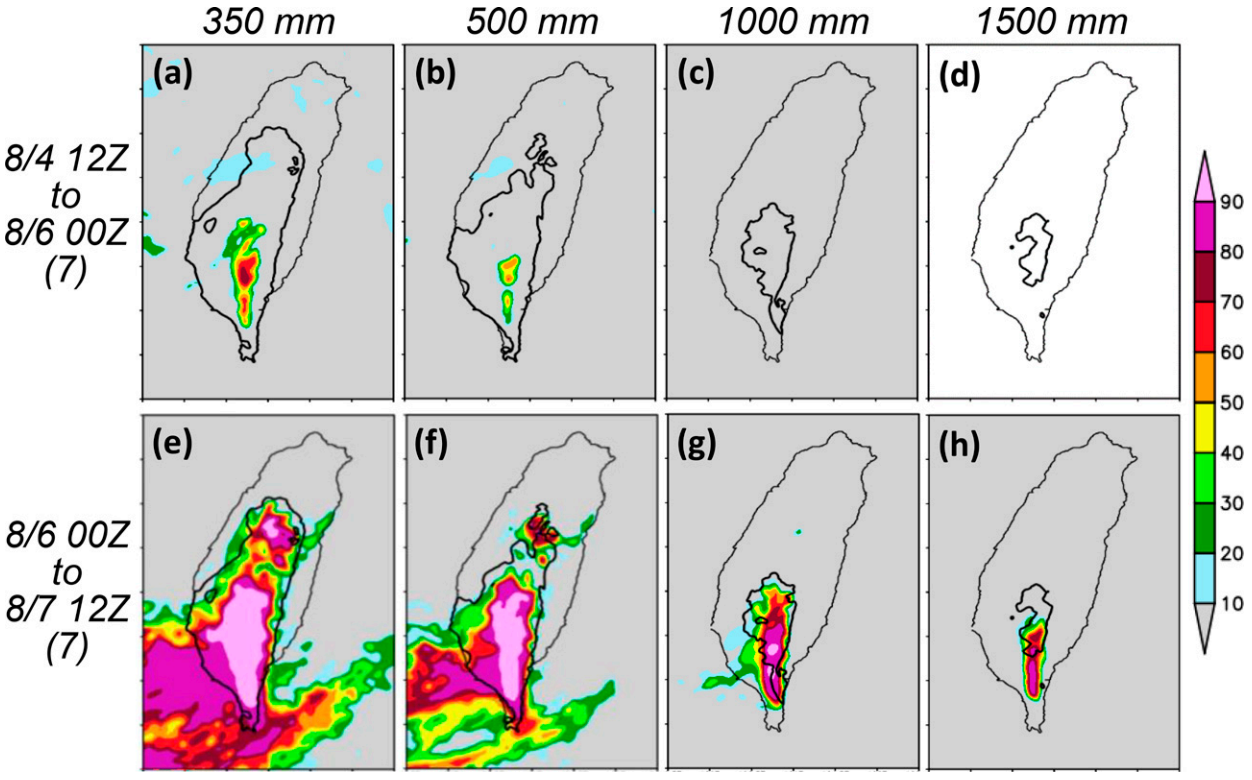

FIG. 11. Probabilities of QPFs (%; color), valid for the 48-h period from 1200 UTC 7 Aug to 1200 UTC 9 Aug, from seven successive time-lagged hindcasts with t_0 between 1200 UTC 4 Aug and 0000 UTC 6 Aug to reach the thresholds of (a) 350, (b) 500, (c) 1000, and (d) 1500 mm, respectively, during TY Morakot (2009). (e)–(h) As in (a)–(d), but from the seven hindcasts with t_0 between 0000 UTC 6 Aug and 1200 UTC 7 Aug 2009. The observed areas (over land) at each respective threshold are depicted by the thick black contours. For each group, the weights assigned to each member are 1/28, 2/28, …, 7/28, from the earliest to the latest, with a total weight of 1 (adapted from Fig. 8 of Wang et al. 2022).

Tied to the topography, the phase-locked LH to/near the terrain can act to "attract" TCs and lengthen the duration of rainfall impact, which has been confirmed by climatological analysis (Fig. 7). Indeed, the slow translation speed (and relatively weak inner-core intensity) of Morakot (Figs. 2 and 5) made it particularly susceptible to the LH effect associated with the extreme rainfall. In summary, the Morakot heavy rainfall event, especially during the exit phase on 8 August, was a result of strong positive feedback and interaction among a weak steering flow (for longer duration), strong low-level southwesterly flow (for moisture supply), asymmetric rainfall and LH (for further slowdown), and the topography (for rainfall/LH enhancement). Whether the cause of the asymmetry is the topography or not, special attention should be paid to such a feedback mechanism in future TC cases in Taiwan to provide early warnings of heavy rainfall.

A few other factors have also been investigated and identified, and they include:

- The large size of Morakot with strong outer circulation: This vortex structure of a TC over northern Taiwan could have contributed to an increased rainfall in the southern CMR region.
- Existence of TS Goni to the west of Morakot: Goni is considered to have strengthened and channeled the southwesterly flow toward southern Taiwan, and is estimated to have contributed about 25% of the peak rainfall of Morakot.
- Warm ocean eddy: The warm ocean eddy, over which Morakot passed over on 6 August, is estimated to have contributed about 10% to the rainfall via increased enthalpy flux.
- Back-building and merging behavior of convective cells inside the quasi-stationary E–W rainband: The interaction between the westerly LLJ in the environment and convective updrafts generated an upward-directed perturbation pressure gradient force that led to an enhancement of updrafts to the rear (west) side and a slowdown of mature cells (Fig. 8). This slowdown would promote merging of mature cells with new cells, low-level convergence, and back-building, and the enhancement of cells would increase the rainfall over the plain areas in southwestern Taiwan during Morakot. To properly simulate such interactions among and within storm cells, a cloud-resolving capability is needed (with $\Delta x \leq 1$–2 km in general).

In conclusion, many of the above factors identified to be important in Morakot may also operate in other TCs and thus contribute to increased rainfall in the WNP and perhaps in TCs around the world, such as the effects by asymmetric LH on storm motion. Islands and coastal regions with steep

topography like Taiwan are particularly vulnerable to extreme rainfall, such as the Philippines (e.g., Bagtasa 2017; Macalalad et al. 2021), Vietnam (e.g., T.-C. Chen et al. 2017), and Japan (e.g., Normile 2019; Titley et al. 2021) in the WNP, as well as Hawaii (e.g., Cullinane 2018; Nugent et al. 2020), India and Sri Lanka (e.g., Krishnamurthy et al. 2018), Madagascar (e.g., Titley et al. 2021), La Réunion (e.g., Pohl et al. 2016), and many Caribbean islands (e.g., Beven and Blake 2015; Hartfield et al. 2018).

In the second section of this review, modeling studies, including forecast and hindcast studies, were reviewed to understand the predictability of Morakot from the standpoint of numerical weather prediction and hazard reduction. The present-day state-of-the-art regional models, configured properly and provided with accurate IC/BCs, could certainly simulate the Morakot rainfall event realistically. For simulations that use analyses as IC/BCs, the initial time can be as early as 3 or 4 August (Fig. 9a), i.e., at least 4–5 days prior to the period of heaviest rainfall in southern Taiwan. An adequate, at least convective-permitting, resolution is necessary for the models to properly simulate most of the finer-scale processes important in Morakot, such as cloud microphysics, asymmetric latent heat release, and orographic effects. A large-enough fine (or inner) domain size is also helpful to better capture the significant cross-scale interactions among these factors and with their background environment. Accordingly, the above configuration is recommended for operational use if such a capability has not yet been established.

However, for real-time forecasts that have larger errors in the BCs at longer lead times, good forecasts of overall Morakot rainfall can only be obtained at lead times within about 2 days. To obtain forecasts with a longer lead time, the ensemble approach is recommended, and a more advanced DA method could also improve the results. Overall, realistic QPFs can be obtained prior to the Morakot event, even though it was one of the more difficult cases with a relatively low predictability. The combined use of time-lagged strategy in the ensemble has been shown to increase the efficiency of computational resources and provide valuable information on time evolution of rainfall probabilities. With the recent improvements in global model forecasts, as well as improved resolution and inner-domain sizes of regional models, an opportunity exists for improved QPFs for TCs like Morakot (2009). On the other hand, given the above deficit in the lead time to produce realistic QPFs for Morakot in forecasts compared to simulations, how to improve the quality of IC/BCs in global models appears to be an important but potentially challenging task. As studies of Morakot on such aspects have been few (e.g., Xiang et al. 2015), much effort is needed in the near future.

The present review has focused on the meteorological aspects of TY Morakot (2009). After the event, much work has also been done in societal aspects to mitigate the disasters such as Morakot (e.g., Chern 2011; Huang and Chang 2011; WRA 2015), but these societal aspects are beyond the scope of the present review.

Acknowledgments. The constructive and valuable comments from four anonymous reviewers helped improve the presentation and clarity of earlier drafts and are much appreciated. The CWB is acknowledged for providing the observational data used in this study. The present study is funded by the Ministry of Science and Technology (MOST) of Taiwan under Grants MOST 108-2111-M-003-005-MY2, MOST 110-2111-M-003-004, and MOST 111-2111-M-003-005.

Data availability statement. The present work is a review article, and all materials used have been published and can be found in the referenced papers.

REFERENCES

Archambault, H. M., L. F. Bosart, D. Keyser, and J. M. Cordeira, 2013: A climatological analysis of the extratropical flow response to recurring western North Pacific tropical cyclones. *Mon. Wea. Rev.*, **141**, 2325–2346, https://doi.org/10.1175/MWR-D-12-00257.1.

Bagtasa, G., 2017: Contribution of tropical cyclones to rainfall in the Philippines. *J. Climate*, **30**, 3621–3633, https://doi.org/10.1175/JCLI-D-16-0150.1.

Beven, J. L., and E. S. Blake, 2015: Atlantic hurricane season of 2010. *Mon. Wea. Rev.*, **143**, 3329–3353, https://doi.org/10.1175/MWR-D-11-00264.1.

Blake, E. S., T. B. Kimberlain, R. J. Berg, J. P. Cangialosi, and J. L. Beven II, 2013: Tropical cyclone report: Hurricane Sandy (22–29 October 2012). National Hurricane Center Rep. AL182012, 157 pp., https://www.nhc.noaa.gov/data/tcr/AL182012_Sandy.pdf.

Burt, C. C., 2014: World rainfall records for 24- and 48-hour periods. Accessed 9 November 2020, https://www.wunderground.com/blog/weatherhistorian/world-rainfall-records-for-24-and-48hour-periods.html.

Chang, C.-P., T.-C. Yeh, and J.-M. Chen, 1993: Effects of terrain on the surface structure of typhoons over Taiwan. *Mon. Wea. Rev.*, **121**, 734–752, https://doi.org/10.1175/1520-0493(1993)121<0734:EOTOTS>2.0.CO;2.

——, Y.-T. Yang, and H.-C. Kuo, 2013: Large increasing trend of tropical cyclone rainfall in Taiwan and the roles of terrain. *J. Climate*, **26**, 4138–4147, https://doi.org/10.1175/JCLI-D-12-00463.1.

Chanson, H., 2010: The impact of Typhoon Morakot on the southern Taiwan coast. *Shore Beach*, **78**, 33–38.

Chen, B., M. Mu, and X. Qin, 2013: The impact of assimilating dropwindsonde data deployed at different sites on typhoon track forecasts. *Mon. Wea. Rev.*, **141**, 2669–2682, https://doi.org/10.1175/MWR-D-12-00142.1.

Chen, C.-W., K.-L. Fu, and L.-L. Lin, 2013: Investigation and analysis of disasters in central and southern Taiwan due to Typhoon Morakot in 2009 (in Chinese). *J. Soil Water Conserv.*, **45**, 663–682.

Chen, J.-M., and C.-F. Shih, 2012: Association between northward-moving tropical cyclones and southwesterly flows modulated by intraseasonal oscillation. *J. Climate*, **25**, 5072–5087, https://doi.org/10.1175/JCLI-D-11-00264.1.

——, P.-H. Tan, and C.-F. Shih, 2013: Heavy rainfall induced by tropical cyclones across northern Taiwan and associated intraseasonal oscillation modulation. *J. Climate*, **26**, 7992–8007, https://doi.org/10.1175/JCLI-D-12-00692.1.

Chen, S., and Coauthors, 2003: COAMPS version 3 model description: General theory and equations. Naval Research Laboratory Tech. Rep. NRL/PU7500-04-448, 141 pp.

——, and Coauthors, 2013: Performance evaluation of radar and satellite rainfalls for Typhoon Morakot over Taiwan: Are remote-sensing products ready for gauge denial scenario of extreme events? *J. Hydrol.*, **506**, 4–13, https://doi.org/10.1016/j.jhydrol.2012.12.026.

Chen, T.-C., and Coauthors, 2010: The precipitation characteristics of Typhoon Morakot (2009) from radar analyses (in Chinese with English abstract). *Atmos. Sci.*, **38**, 39–61.

——, J.-D. Tsay, and J. Matsumoto, 2017: Interannual variation of the summer rainfall center in the South China Sea. *J. Climate*, **30**, 7909–7931, https://doi.org/10.1175/JCLI-D-16-0889.1.

Chen, Y.-H., H.-C. Kuo, C.-C. Wang, and Y.-T. Yang, 2017: Influence of southwest monsoon flow and typhoon track on Taiwan rainfall during the exit phase: Modeling study of Typhoon Morakot (2009). *Quart. J. Roy. Meteor. Soc.*, **143**, 3014–3024, https://doi.org/10.1002/qj.3156.

Chern, J.-C., 2011: Morakot post-disaster reconstruction in Taiwan. Morakot Post-Disaster Reconstruction Council, Executive Yuan, Taiwan, 152 pp., http://morakotdatabase.nstm.gov.tw/88flood.www.gov.tw/eng/Reconstruction_reports.html#idx1.

Cheung, K. K. W., L.-R. Huang, and C.-S. Lee, 2008: Characteristics of rainfall during tropical cyclone periods in Taiwan. *Nat. Hazards Earth Syst. Sci.*, **8**, 1463–1474, https://doi.org/10.5194/nhess-8-1463-2008.

Chi, S.-S., 2006: The Mei-Yu in Taiwan (in Chinese). Chung-Shin Engineering Technology Research and Development Foundation SFRDEST E-06-MT-03-4, 65 pp.

Chien, F.-C., and H.-C. Kuo, 2011: On the extreme rainfall of Typhoon Morakot (2009). *J. Geophys. Res.*, **116**, D05104, https://doi.org/10.1029/2010JD015092.

Chou, K.-H., C.-C. Wu, P.-H. Lin, S. D. Aberson, M. Weissmann, F. Harnisch, and T. Nakazawa, 2011: The impact of dropwindsonde observations on typhoon track forecasts in DOTSTAR and T-PARC. *Mon. Wea. Rev.*, **139**, 1728–1743, https://doi.org/10.1175/2010MWR3582.1.

Chu, H.-J., T.-Y. Pan, and J.-J. Liou, 2011: Extreme precipitation estimation with Typhoon Morakot using frequency and spatial analysis. *Terr. Atmos. Oceanic Sci.*, **22**, 549–558, https://doi.org/10.3319/TAO.2011.05.10.02(TM).

Corbosiero, K. L., and J. Molinari, 2002: The effects of vertical wind shear on the distribution of convection in tropical cyclones. *Mon. Wea. Rev.*, **130**, 2110–2123, https://doi.org/10.1175/1520-0493(2002)130<2110:TEOVWS>2.0.CO;2.

Cullinane, S., 2018: Hurricane Lane dumped 52 inches of rain on Hawaii and there might be more on the way. *CNN News*, 28 August 2018, https://edition.cnn.com/2018/08/28/us/hawaii-tropical-storm-lane-flooding-wxc/index.html.

Davis, C. A., 1992: Piecewise potential vorticity inversion. *J. Atmos. Sci.*, **49**, 1397–1411, https://doi.org/10.1175/1520-0469(1992)049<1397:PPVI>2.0.CO;2.

——, and K. A. Emanuel, 1991: Potential vorticity diagnostics of cyclogenesis. *Mon. Wea. Rev.*, **119**, 1929–1953, https://doi.org/10.1175/1520-0493(1991)119<1929:PVDOC>2.0.CO;2.

——, B. Brown, and R. Bullock, 2006: Object-based verification of precipitation forecasts. Part I: Methodology and application to mesoscale rain areas. *Mon. Wea. Rev.*, **134**, 1772–1784, https://doi.org/10.1175/MWR3145.1.

Ding, Y., and J. C.-L. Chan, 2005: The East Asian summer monsoon: An overview. *Meteor. Atmos. Phys.*, **89**, 117–142, https://doi.org/10.1007/s00703-005-0125-z.

Doswell, C. A., III, H. E. Brooks, and R. A. Maddox, 1996: Flash flood forecasting: An ingredients-based methodology. *Wea. Forecasting*, **11**, 560–581, https://doi.org/10.1175/1520-0434(1996)011<0560:FFFAIB>2.0.CO;2.

Dudhia, J., D. Gill, K. Manning, W. Wang, and C. Bruyere, 2005: PSU/NCAR mesoscale modeling system tutorial class notes and user's guide: MM5 Modeling System version 3. Mesoscale and Microscale Meteorology Division, National Center for Atmospheric Research, Boulder, CO, 324 pp., https://vdoc.pub/documents/psu-ncar-mesoscale-modeling-system-tutorial-class-notes-and-users-guide-mm5-modeling-system-version-3-2jv1v7bpt390.

Ebert, E. E., and J. L. McBride, 2000: Verification of precipitation in weather systems: Determination of systematic errors. *J. Hydrol.*, **239**, 179–202, https://doi.org/10.1016/S0022-1694(00)00343-7.

——, M. Turk, S. J. Kusselson, J. Yang, M. Seybold, P. R. Keehn, and R. J. Kuligowski, 2011: Ensemble Tropical Rainfall Potential (eTRaP) forecasts. *Wea. Forecasting*, **26**, 213–224, https://doi.org/10.1175/2010WAF2222443.1.

Emanuel, K. A., 2005: Increasing destructiveness of tropical cyclones over the past 30 years. *Nature*, **436**, 686–688, https://doi.org/10.1038/nature03906.

Evans, C., and Coauthors, 2017: The extratropical transition of tropical cyclones. Part I: Cyclone evolution and direction impacts. *Mon. Wea. Rev.*, **145**, 4317–4344, https://doi.org/10.1175/MWR-D-17-0027.1.

Fang, X., and Y.-H. Kuo, 2013: Improving ensemble-based quantitative precipitation forecasts for topography-enhanced typhoon heavy rainfall over Taiwan with a modified probability-matching technique. *Mon. Wea. Rev.*, **141**, 3908–3932, https://doi.org/10.1175/MWR-D-13-00012.1.

——, ——, and A. Wang, 2011: The impact of Taiwan topography on the predictability of Typhoon Morakot's record-breaking rainfall: A high-resolution ensemble simulation. *Wea. Forecasting*, **26**, 613–633, https://doi.org/10.1175/WAF-D-10-05020.1.

Feng, L., P.-L. Chang, and B. J.-D. Jou, 2012: The relationships between the upstream wind and orographic heavy rainfall in southwestern Taiwan for typhoon cases. *IAHS Publ.*, **351**, 287–292.

Fernández-Cabán, P. L., and Coauthors, 2019: Observing Hurricane Harvey's eyewall at landfall. *Bull. Amer. Meteor. Soc.*, **100**, 759–775, https://doi.org/10.1175/BAMS-D-17-0237.1.

Fujiwhara, S., 1921: The mutual tendency towards symmetry of motion and its application as a principle in meteorology. *Quart. J. Roy. Meteor. Soc.*, **47**, 287–293, https://doi.org/10.1002/qj.49704720010.

Galarneau, T. J., Jr., C. A. Davis, and M. A. Shapiro, 2013: Intensification of Hurricane Sandy (2012) through extratropical warm core seclusion. *Mon. Wea. Rev.*, **141**, 4296–4321, https://doi.org/10.1175/MWR-D-13-00181.1.

Ge, X., T. Li, S. Zhang, and M. S. Peng, 2010: What causes the extremely heavy rainfall in Taiwan during Typhoon Morakot (2009)? *Atmos. Sci. Lett.*, **11**, 46–50, https://doi.org/10.1002/asl.255.

Hall, J.-D., M. Xue, L. Ran, and L.-M. Leslie, 2013: High-resolution modeling of Typhoon Morakot (2009): Vortex Rossby waves and their role in extreme precipitation over Taiwan. *J. Atmos. Sci.*, **70**, 163–186, https://doi.org/10.1175/JAS-D-11-0338.1.

Hamill, T. M., J. S. Whitaker, M. Fiorino, and S. G. Benjamin, 2011: Global ensemble predictions of 2009's tropical cyclones initialized with an ensemble Kalman filter. *Mon. Wea. Rev.*, **139**, 668–688, https://doi.org/10.1175/2010MWR3456.1.

Hartfield, G., J. Blunden, and D. S. Arndt, 2018: A look at 2017: Takeaway points from the *State of the Climate* supplement.

Bull. Amer. Meteor. Soc., **99**, 1527–1539, https://doi.org/10.1175/BAMS-D-18-0173.1.

Hendricks, E. A., J. R. Moskaitis, Y. Jin, R. M. Hodur, J. D. Doyle, and M. S. Peng, 2011: Prediction and diagnosis of Typhoon Morakot (2009) using the Naval Research Laboratory's mesoscale tropical cyclone model. *Terr. Atmos. Oceanic Sci.*, **22**, 579–594, https://doi.org/10.3319/TAO.2011.05.30.01(TM).

——, Y. Jin, J. R. Moskaitis, J. D. Doyle, M. S. Peng, C.-C. Wu, and H.-C. Kuo, 2016: Numerical simulations of Typhoon Morakot (2009) using a multiply nested tropical cyclone prediction model. *Wea. Forecasting*, **31**, 627–645, https://doi.org/10.1175/WAF-D-15-0016.1.

Hodur, R. M., 1997: The Naval Research Laboratory's Coupled Ocean/Atmosphere Mesoscale Prediction System (COAMPS). *Mon. Wea. Rev.*, **125**, 1414–1430, https://doi.org/10.1175/1520-0493(1997)125<1414:TNRLSC>2.0.CO;2.

Hong, C.-C., M.-Y. Lee, H.-H. Hsu, and J.-L. Kuo, 2010: Role of submonthly disturbance and 40-50 day ISO on the extreme rainfall event associated with Typhoon Morakot (2009) in southern Taiwan. *Geophys. Res. Lett.*, **37**, L08805, https://doi.org/10.1029/2010GL042761.

Hoover, B. T., and M. C. Morgan, 2011: Dynamical sensitivity analysis of tropical cyclone steering using an adjoint model. *Mon. Wea. Rev.*, **139**, 2761–2775, https://doi.org/10.1175/MWR-D-10-05084.1.

Hsu, H.-H., H.-C. Kuo, J.-D. Jou, T.-C. Chen, P.-H. Lin, T.-C. Yeh, and C.-C. Wu, 2010: *Scientific Report on Typhoon Morakot (2009) (in Chinese)*. National Science Council, 192 pp.

Hsu, L.-H., H.-C. Kuo, and R. G. Fovell, 2013: On the geographic asymmetry of typhoon translation speed across the mountainous island of Taiwan. *J. Atmos. Sci.*, **70**, 1006–1022, https://doi.org/10.1175/JAS-D-12-0173.1.

Huang, C.-Y., and T.-Y. Chao, 2013: Rainfall simulation associated with Typhoon Morakot (2009) (in Chinese with English abstract). *Atmos. Sci.*, **41**, 91–115.

——, C.-S. Wong, and T.-C. Yeh, 2011: Extreme rainfall mechanisms exhibited by Typhoon Morakot (2009). *Terr. Atmos. Oceanic Sci.*, **22**, 613–632, https://doi.org/10.3319/TAO.2011.07.01.01(TM).

——, Y. Zhang, W. C. Skamarock, and L.-H. Hsu, 2017: Influences of large-scale flow variations on the track evolution of Typhoons Morakot (2009) and Megi (2010): Simulations with a global variable-resolution model. *Mon. Wea. Rev.*, **145**, 1691–1716, https://doi.org/10.1175/MWR-D-16-0363.1.

Huang, H.-L., M.-J. Yang, and C.-H. Sui, 2014: Water budget and precipitation efficiency of Typhoon Morakot (2009). *J. Atmos. Sci.*, **71**, 112–129, https://doi.org/10.1175/JAS-D-13-053.1.

Huang, J. J., and W. R. Chang, 2011: Policy progress in mitigation of climate change in Taiwan. *Energy Policy*, **39**, 1113–1122, https://doi.org/10.1016/j.enpol.2010.11.033.

Huang, Y.-C., and Y.-L. Lin, 2014: A study on the structure and precipitation of Morakot (2009) induced by the Central Mountain Range of Taiwan. *Meteor. Atmos. Phys.*, **123**, 115–141, https://doi.org/10.1007/s00703-013-0290-4.

Jang, W., and H.-Y. Chun, 2015: Characteristics of binary tropical cyclones observed in the western North Pacific for 62 years (1951–2012). *Mon. Wea. Rev.*, **143**, 1749–1761, https://doi.org/10.1175/MWR-D-14-00331.1.

Johnson, R. H., and B. E. Mapes, 2001: Mesoscale processes and severe convective weather. *Severe Convective Storms Meteor. Monogr.*, No. 50, Amer. Meteor. Soc., 71–122.

Jou, B. J.-D., Y.-C. Yu, L. Feng, Y.-M. Chen, C.-S. Lee, and M.-D. Cheng, 2010: Synoptic environment and rainfall characteristics of Typhoon Morakot (0908) (in Chinese with English abstract). *Atmos. Sci.*, **38**, 21–38.

Klemp, J. B., 1987: Dynamics of tornadic thunderstorms. *Annu. Rev. Fluid Mech.*, **19**, 369–402, https://doi.org/10.1146/annurev.fl.19.010187.002101.

Knutson, T. R., and Coauthors, 2010: Tropical cyclones and climate change. *Nat. Geosci.*, **3**, 157–163, https://doi.org/10.1038/ngeo779.

Krishnamurthy, L., and Coauthors, 2018: Causes and probability of occurrence of extreme precipitation events like Chennai 2015. *J. Climate*, **31**, 3831–3848, https://doi.org/10.1175/JCLI-D-17-0302.1.

Kuo, H.-C., G. T.-J. Chen, and C.-H. Lin, 2000: Merger of Tropical Cyclones Zeb and Alex. *Mon. Wea. Rev.*, **128**, 2967–2975, https://doi.org/10.1175/1520-0493(2000)128<2967:MOTCZA>2.0.CO;2.

——, and Coauthors, 2012: *Typhoon Prevention and Hazard Reduction* (in Chinese). Meteorological Application and Outreach Foundation, 138 pp.

Kuo, Y.-C., Z.-W. Zheng, Q. Zheng, G. Gopalakrishnan, and H.-Y. Lee, 2018: Typhoon– Kuroshio interaction in an air–sea coupled system: Case study of Typhoon Nanmadol (2011). *Ocean Modell.*, **132**, 130–138, https://doi.org/10.1016/j.ocemod.2018.10.007.

Kuo, Y.-H., and G. T.-J. Chen, 1990: The Taiwan Area Mesoscale Experiment (TAMEX): An overview. *Bull. Amer. Meteor. Soc.*, **71**, 488–503, https://doi.org/10.1175/1520-0477(1990)071<0488:TTAMEA>2.0.CO;2.

Kuo, Y.-M., H.-J. Chu, and T.-Y. Pan, 2014: Temporal precipitation estimation from nearby radar reflectivity using dynamic factor analysis in the mountainous watershed—A case during Typhoon Morakot. *Hydrol. Processes*, **28**, 999–1008, https://doi.org/10.1002/hyp.9639.

Lackmann, G. M., 2015: Hurricane Sandy before 1900 and after 2100. *Bull. Amer. Meteor. Soc.*, **96**, 547–559, https://doi.org/10.1175/BAMS-D-14-00123.1.

Lander, M. A., 1994: Description of a monsoon gyre and its effect on the tropical cyclones in the Western North Pacific during August 1991. *Wea. Forecasting*, **9**, 640–654, https://doi.org/10.1175/1520-0434(1994)009<0640:DOAMGA>2.0.CO;2.

Lee, C.-S., C.-C. Wu, T.-C. Chen, and R. L. Elsberry, 2011: Advances in understanding the "perfect monsoon-influenced typhoon": Summary from international conference on typhoon Morakot (2009). *Asia-Pac. J. Atmos. Sci.*, **47**, 213–222, https://doi.org/10.1007/s13143-011-0010-2.

Lee, H. S., T. Yamashita, J. R.-C. Hsu, and F. Ding, 2013: Integrated modeling of the dynamic meteorological and sea surface conditions during the passage of Typhoon Morakot. *Dyn. Atmos. Oceans*, **59**, 1–23, https://doi.org/10.1016/j.dynatmoce.2012.09.002.

Liang, J., and L. Wu, 2015: Sudden track changes of tropical cyclones in monsoon gyres: Full-physics, idealized numerical experiments. *J. Atmos. Sci.*, **72**, 1307–1322, https://doi.org/10.1175/JAS-D-13-0393.1.

——, ——, X. Ge, and C.-C. Wu, 2011: Monsoonal influence on Typhoon Morakot (2009). Part II: Numerical study. *J. Atmos. Sci.*, **68**, 2222–2235, https://doi.org/10.1175/2011JAS3731.1.

Lin, C.-Y., H.-M. Hsu, Y.-F. Sheng, C.-H. Kuo, and Y.-A. Liou, 2011: Mesoscale processes for super heavy rainfall of Typhoon Morakot (2009) over southern Taiwan. *Atmos. Chem. Phys.*, **11**, 345–361, https://doi.org/10.5194/acp-11-345-2011.

Lin, I.-I., C.-H. Chen, I.-F. Pun, W. T. Liu, and C.-C. Wu, 2009: Warm ocean anomaly, air sea fluxes, and the rapid intensification of Tropical Cyclone Nargis (2008). *Geophys. Res. Lett.*, **36**, L03817, https://doi.org/10.1029/2008GL035815.

——, M.-D. Chou, and C.-C. Wu, 2011: The impact of a warm ocean eddy on Typhoon Morakot (2009): A preliminary study from satellite observations and numerical modeling. *Terr. Atmos. Oceanic Sci.*, **22**, 661–671, https://doi.org/10.3319/TAO.2011.08.19.01(TM).

Lin, Y.-L., S. Chiao, T.-A. Wang, and M. L. Kaplan, 2001: Some common ingredients for heavy orographic rainfall. *Wea. Forecasting*, **16**, 633–660, https://doi.org/10.1175/1520-0434(2001)016<0633:SCIFHO>2.0.CO;2.

Liou, Y.-C., T.-C. Chen Wang, Y.-C. Tsai, Y.-S. Tang, P.-L. Lin, and Y.-A. Lee, 2013: Structure of precipitating systems over Taiwan's complex terrain during Typhoon Morakot (2009) as revealed by weather radar and rain gauge observations. *J. Hydrol.*, **506**, 14–25, https://doi.org/10.1016/j.jhydrol.2012.09.004.

——, ——, and P.-Y. Huang, 2016: The inland eyewall reintensification of Typhoon Fanapi (2010) documented from an observational perspective using multiple-Doppler radar and surface measurements. *Mon. Wea. Rev.*, **144**, 241–261, https://doi.org/10.1175/MWR-D-15-0136.1.

Liu, C.-C., G.-R. Liu, T.-H. Lin, and C.-C. Chao, 2010: Accumulated rainfall forecast of Typhoon Morakot (2009) in Taiwan using satellite data. *J. Meteor. Soc. Japan*, **88**, 785–798, https://doi.org/10.2151/jmsj.2010-501.

Liu, Z., D. Ostrenga, W. Teng, and S. Kempler, 2012: Tropical Rainfall Measuring Mission (TRMM) precipitation data and services for research and applications. *Bull. Amer. Meteor. Soc.*, **93**, 1317–1325, https://doi.org/10.1175/BAMS-D-11-00152.1.

Macalalad, R. V., R. A. Badilla, O. C. Cabrera, and G. Bagtasa, 2021: Hydrological response of the Pampanga River basin in the Philippines to intense tropical cyclone rainfall. *J. Hydrometeor.*, **22**, 781–794, https://doi.org/10.1175/JHM-D-20-0184.1.

Marks, F. D., and L. K. Shay, 1998: Landfalling tropical cyclones: Forecast problems and associated research opportunities. *Bull. Amer. Meteor. Soc.*, **79**, 305–323, https://doi.org/10.1175/1520-0477(1998)079<0305:LTCFPA>2.0.CO;2.

McPhaden, M. J., and Coauthors, 2009: Ocean-atmosphere interactions during cyclone Nargis. *Eos, Trans. Amer. Geophys. Union*, **90**, 53–54, https://doi.org/10.1029/2009EO070001.

McTaggart-Cowan, R., L. F. Bosart, J. R. Gyakum, and E. H. Atallah, 2007: Hurricane Katrina (2005). Part I: Complex life cycle of an intense tropical cyclone. *Mon. Wea. Rev.*, **135**, 3905–3926, https://doi.org/10.1175/2007MWR1875.1.

Ming, J., and J. A. Zhang, 2016: Effects of surface flux parameterization on the numerically simulated intensity and structure of Typhoon Morakot (2009). *Adv. Atmos. Sci.*, **33**, 58–72, https://doi.org/10.1007/s00376-015-4202-z.

Nguyen, H. V., and Y.-L. Chen, 2011: High resolution initialization and simulations of Typhoon Morakot (2009). *Mon. Wea. Rev.*, **139**, 1463–1491, https://doi.org/10.1175/2011MWR3505.1.

——, and ——, 2014: Improvements to a tropical cyclone initialization scheme and impacts on forecasts. *Mon. Wea. Rev.*, **142**, 4340–4356, https://doi.org/10.1175/MWR-D-13-00326.1.

Normile, D., 2019: Deadly typhoon forces Japan to face its vulnerability to increasingly powerful storms. *ScienceInsider*, 22 October 2019, https://www.science.org/content/article/deadly-typhoon-forces-japan-face-its-vulnerability-increasingly-powerful-storms.

Nugent, A. D., R. J. Longman, C. Trauernicht, M. P. Lucas, H. F. Diaz, and T. W. Giambelluca, 2020: Fire and rain: The legacy of hurricane lane in Hawai'i. *Bull. Amer. Meteor. Soc.*, **101**, E954–E967, https://doi.org/10.1175/BAMS-D-19-0104.1.

Petley, D., 2010: The causes of the Shiaolin landslide disaster in Taiwan. The Landslide Blog, accessed 30 November 2021, https://blogs.agu.org/landslideblog/2010/02/02/the-causes-of-the-shiaolin-landslide-disaster-in-taiwan/.

Pohl, B., B. Morel, C. Barthe, and O. Bousquet, 2016: Regionalizing rainfall at very high resolution over La Réunion Island: A case study for Tropical Cyclone Ando. *Mon. Wea. Rev.*, **144**, 4081–4099, https://doi.org/10.1175/MWR-D-15-0404.1.

Qin, X., and M. Mu, 2011: A study on the reduction of forecast error variance by three adaptive observation approaches for tropical cyclone prediction. *Mon. Wea. Rev.*, **139**, 2218–2232, https://doi.org/10.1175/2010MWR3327.1.

Rogers, R., and Coauthors, 2013: NOAA's Hurricane Intensity Forecasting Experiment: A progress report. *Bull. Amer. Meteor. Soc.*, **94**, 859–882, https://doi.org/10.1175/BAMS-D-12-00089.1.

Rotunno, R., and J. B. Klemp, 1982: The influence of the shear-induced pressure gradient on thunderstorm motion. *Mon. Wea. Rev.*, **110**, 136–151, https://doi.org/10.1175/1520-0493(1982)110<0136:TIOTSI>2.0.CO;2.

Schaefer, J. T., 1990: The critical success index as an indicator of warning skill. *Wea. Forecasting*, **5**, 570–575, https://doi.org/10.1175/1520-0434(1990)005<0570:TCSIAA>2.0.CO;2.

Schwartz, C. S., Z. Liu, Y. Chen, and X.-Y. Huang, 2012: Impact of assimilating microwave radiances with a limited-area ensemble data assimilation system on forecasts of Typhoon Morakot. *Wea. Forecasting*, **27**, 424–437, https://doi.org/10.1175/WAF-D-11-00033.1.

Skamarock, W. C., J. B. Klemp, J. Dudhia, D. O. Gill, D. M. Barker, W. Wang, and J. G. Powers, 2005: A description of the Advanced Research WRF version 2. NCAR Tech. Note NCAR/TN-468+STR, 88 pp., https://doi.org/10.5065/D6DZ069T.

Smith, R. K., M. T. Montgomery, and V. S. Nguyen, 2009: Tropical cyclone spin-up revisited. *Quart. J. Roy. Meteor. Soc.*, **135**, 1321–1335, https://doi.org/10.1002/qj.428.

Soria, J. L. A., and Coauthors, 2016: Repeat storm surge disasters of Typhoon Haiyan and its 1897 predecessor in the Philippines. *Bull. Amer. Meteor. Soc.*, **97**, 31–48, https://doi.org/10.1175/BAMS-D-14-00245.1.

Su, S.-H., H.-C. Kuo, L.-H. Hsu, and Y.-T. Yang, 2012: Temporal and spatial characteristics of typhoon extreme rainfall in Taiwan. *J. Meteor. Soc. Japan*, **90**, 721–736, https://doi.org/10.2151/jmsj.2012-510.

——, Y.-H. Chen, Y.-T. Yang, L.-H. Hsu, and H.-C. Kuo, 2017: The mechanism of Taiwan typhoon extreme rainfall variation under climate change (in Chinese with English abstract). *Atmos. Sci.*, **45**, 305–331.

Taniguchi, A., and Coauthors, 2013: Improvement of high-resolution satellite rainfall product for Typhoon Morakot (2009) over Taiwan. *J. Hydrometeor.*, **14**, 1859–1871, https://doi.org/10.1175/JHM-D-13-047.1.

Tao, W.-K., and Coauthors, 2011: High-resolution numerical simulation of the extreme rainfall associated with Typhoon Morakot. Part I: Comparing the impact of microphysics and PBL parameterizations with observations. *Terr. Atmos. Oceanic Sci.*, **22**, 673–696, https://doi.org/10.3319/TAO.2011.08.26.01(TM).

Taylor, K. E., R. J. Stouffer, and G. A. Meehl, 2012: An overview of CMIP5 and the experiment design. *Bull. Amer. Meteor. Soc.*, **93**, 485–498, https://doi.org/10.1175/BAMS-D-11-00094.1.

Titley, H. A., H. L. Cloke, S. Harrigan, F. Pappenberger, C. Prudhomme, J. C. Robbins, E. M. Stephens, and E. Zsótér, 2021: Key factors influencing the severity of fluvial flood hazard from tropical cyclones. *J. Hydrometeor.*, **22**, 1801–1817, https://doi.org/10.1175/JHM-D-20-0250.1.

Tsuboki, K., and A. Sakakibara, 2002: Large-scale parallel computing of cloud resolving storm simulator. *High Performance Computing*, H. P. Zima et al., Eds., Springer, 243–259.

——, and ——, 2007: *Numerical Prediction of High-Impact Weather Systems: The Textbook for Seventeenth IHP Training Course in 2007*, Nagoya University and UNESCO, 273 pp.

Wang, B., Ed., 2006: *The Asian Monsoon*. Springer-Praxis, 787 pp.

Wang, C.-C., 2014: On the calculation and correction of equitable threat score for model quantitative precipitation forecasts for small verification areas: The example of Taiwan. *Wea. Forecasting*, **29**, 788–798, https://doi.org/10.1175/WAF-D-13-00087.1.

——, H.-C. Kuo, Y.-H. Chen, H.-L. Huang, C.-H. Chung, and K. Tsuboki, 2012: Effects of asymmetric latent heating on typhoon movement crossing Taiwan: The case of Morakot (2009) with extreme rainfall. *J. Atmos. Sci.*, **69**, 3172–3196, https://doi.org/10.1175/JAS-D-11-0346.1.

——, Y.-H. Chen, H.-C. Kuo, and S.-Y. Huang, 2013a: Sensitivity of typhoon track to asymmetric latent heating/rainfall induced by Taiwan topography: A numerical study of Typhoon Fanapi (2010). *J. Geophys. Res. Atmos.*, **118**, 3292–3308, https://doi.org/10.1002/jgrd.50351.

——, H.-C. Kuo, T.-C. Yeh, C.-H. Chung, Y.-H. Chen, S.-Y. Huang, Y.-W. Wang, and C.-H. Liu, 2013b: High-resolution quantitative precipitation forecasts and simulations by the Cloud-Resolving Storm Simulator (CReSS) for Typhoon Morakot (2009). *J. Hydrol.*, **506**, 26–41, https://doi.org/10.1016/j.jhydrol.2013.02.018.

——, ——, R. H. Johnson, C.-Y. Lee, S.-Y. Huang, and Y.-H. Chen, 2015: A numerical study of convection in rainbands of Typhoon Morakot (2009) with extreme rainfall: Roles of pressure perturbations with low-level wind maxima. *Atmos. Chem. Phys.*, **15**, 11 097–11 115, https://doi.org/10.5194/acp-15-11097-2015.

——, S.-Y. Huang, S.-H. Chen, C.-S. Chang, and K. Tsuboki, 2016: Cloud-resolving typhoon rainfall ensemble forecasts for Taiwan with large domain and extended range through time-lagged approach. *Wea. Forecasting*, **31**, 151–172, https://doi.org/10.1175/WAF-D-15-0045.1.

——, L.-S. Tseng, C.-C. Huang, S.-H. Lo, C.-T. Chen, P.-Y. Chuang, and N.-C. Su, 2019: How much of Typhoon Morakot's extreme rainfall is attributable to anthropogenic climate change? *Int. J. Climatol.*, **39**, 3454–3464, https://doi.org/10.1002/joc.6030.

——, K.-Y. Lin, C. A. Davis, S.-Y. Huang, S. C.-S. Liu, K. Tsuboki, and B. J.-D. Jou, 2020: A modeling study on the impacts of Typhoon Morakot's (2009) vortex structure on rainfall in Taiwan using piecewise potential vorticity inversion. *J. Meteor. Soc. Japan*, **98**, 707–733, https://doi.org/10.2151/jmsj.2020-036.

——, Y.-H. Chen, M.-C. Li, H.-C. Kuo, and K. Tsuboki, 2021: On the separation of upper and low-level centres of Tropical Storm Kong-Rey (2013) near Taiwan in association with asymmetric latent heating. *Quart. J. Roy. Meteor. Soc.*, **147**, 1135–1149, https://doi.org/10.1002/qj.3963.

——, S.-H. Chen, K. Tsuboki, S.-Y. Huang, and C.-S. Chang, 2022: Application of time-lagged ensemble quantitative precipitation forecasts for Typhoon Morakot (2009) in Taiwan by a cloud-resolving model. *Atmosphere*, **13**, 585, https://doi.org/10.3390/atmos13040585.

Wang, S.-T., 1989: Track, intensity, structure, wind and precipitation characteristics of typhoons affecting Taiwan (in Chinese). National Science Council of Taiwan Disaster Mitigation Research Rep. 80-73, NSC 80-04140-P052-02B, 285 pp.

Webster, P. J., 2008: Myanmar's deadly "daffodil." *Nat. Geosci.*, **1**, 488–490, https://doi.org/10.1038/ngeo257.

Wei, C.-H., T.-H. Hor, Y.-C. Chuang, T.-C. Chen Wang, and J.-L. Wang, 2012: Radar analysis on the interaction between southwesterly monsoonal flow and circulation associated with Typhoon Morakot (2009). *J. Meteor. Soc. Japan*, **90**, 617–628, https://doi.org/10.2151/jmsj.2012-503.

——, Y.-C. Chuang, T.-H. Hor, C.-C. Liao, and N.-C. Yeh, 2014: Dual-Doppler radar investigation of a convective rainband during the impact of the southwesterly monsoonal flow on the circulation of Typhoon Morakot (2009). *J. Meteor. Soc. Japan*, **92**, 363–383, https://doi.org/10.2151/jmsj.2014-406.

Wilks, D. S., 1995: *Statistical Methods in the Atmospheric Sciences: An Introduction*. International Geophysics Series, Vol. 59, Elsevier, 467 pp.

WRA, 2015: The application of multi-hazard mitigation and prevention technology in Taiwan. Water Resources Agency, Ministry of Economic Affairs, ROC, accessed 30 November 2021, https://slideplayer.com/slide/8173820/.

Wu, C.-C., 2013: Typhoon Morakot: Key findings from the journal *TAO* for improving prediction of extreme rains at landfall. *Bull. Amer. Meteor. Soc.*, **94**, 155–160, https://doi.org/10.1175/BAMS-D-11-00155.1.

——, and Y.-H. Kuo, 1999: Typhoons affecting Taiwan: Current understanding and future challenges. *Bull. Amer. Meteor. Soc.*, **80**, 67–80, https://doi.org/10.1175/1520-0477(1999)080<0067:TATCUA>2.0.CO;2.

——, T.-S. Huang, W.-P. Huang, and K.-H. Chou, 2003: A new look at the binary interaction: Potential vorticity diagnosis of the unusual southward movement of Tropical Storm Bopha (2000) and its interaction with Supertyphoon Saomai (2000). *Mon. Wea. Rev.*, **131**, 1289–1300, https://doi.org/10.1175/1520-0493(2003)131<1289:ANLATB>2.0.CO;2.

——, and Coauthors, 2005: Dropwindsonde Observations for Typhoon Surveillance near the Taiwan Region (DOTSTAR): An overview. *Bull. Amer. Meteor. Soc.*, **86**, 787–794, https://doi.org/10.1175/BAMS-86-6-787.

——, C.-Y. Huang, M.-J. Yang, F.-C. Chien, J.-S. Hong, and T.-H. Yen, 2010: Typhoon Morakot (2009) and a special review on the current status and future challenge of tropical cyclone simulation (in Chinese with English abstract). *Atmos. Sci.*, **38**, 99–134.

Wu, C.-H., S.-C. Chen, and Z.-Y. Feng, 2014: Formation, failure, and consequences of the Xiaolin landslide dam, triggered by extreme rainfall from Typhoon Morakot, Taiwan. *Landslides*, **11**, 357–367, https://doi.org/10.1007/s10346-013-0394-4.

Wu, L., and B. Wang, 2000: A potential vorticity tendency diagnostic approach for tropical cyclone motion. *Mon. Wea. Rev.*, **128**, 1899–1911, https://doi.org/10.1175/1520-0493(2000)128<1899:APVTDA>2.0.CO;2.

——, J. Liang, and C.-C. Wu, 2011: Monsoonal influence on Typhoon Morakot (2009). Part I: Observational analysis. *J. Atmos. Sci.*, **68**, 2208–2221, https://doi.org/10.1175/2011JAS3730.1.

——, Z. Ni, J. Duan, and H. Zong, 2013: Sudden tropical cyclone track changes over the western North Pacific: A composite study. *Mon. Wea. Rev.*, **141**, 2597–2610, https://doi.org/10.1175/MWR-D-12-00224.1.

Xiang, B., and Coauthors, 2015: Beyond weather time-scale prediction for Hurricane Sandy and Super Typhoon Haiyan in a global climate model. *Mon. Wea. Rev.*, **143**, 524–535, https://doi.org/10.1175/MWR-D-14-00227.1.

Xie, B., and F. Zhang, 2012: Impacts of typhoon track and island topography on the heavy rainfalls in Taiwan associated with Morakot (2009). *Mon. Wea. Rev.*, **140**, 3379–3394, https://doi.org/10.1175/MWR-D-11-00240.1.

——, ——, Q. Zhang, J. Poterjoy, and Y. Weng, 2013: Observing strategy and observation targeting for tropical cyclones using ensemble-based sensitivity analysis and data assimilation. *Mon. Wea. Rev.*, **141**, 1437–1453, https://doi.org/10.1175/MWR-D-12-00188.1.

Xu, Y., and X. Lu, 2014: Numerical experimental study for the effect of a binary typhoon system on the extreme rainfall of Typhoon Morakot (0908). *Trop. Cyclone Res. Rev.*, **3**, 35–43, https://doi.org/10.6057/2014TCRR01.03.

Xue, M., K. K. Droegemeier, and V. Wong, 2000: The Advanced Regional Prediction System (ARPS)—A multiscale nonhydrostatic atmospheric simulation and prediction tool. Part I: Model dynamics and verification. *Meteor. Atmos. Phys.*, **75**, 161–193, https://doi.org/10.1007/s007030070003.

——, and Coauthors, 2001: The Advanced Regional Prediction System (ARPS)—A multiscale nonhydrostatic atmospheric simulation and prediction tool. Part II: Model physics and applications. *Meteor. Atmos. Phys.*, **76**, 143–165, https://doi.org/10.1007/s007030170027.

Yang, Y.-M., M.-B. Du, and J. Zhang, 2013: FY-3A satellite microwave data assimilation experiments in tropical cyclone forecast. *J. Trop. Meteor.*, **19**, 297–304.

Yeh, T.-C., H.-C. Kuo, K.-C. Lu, S.-C. Wang, and Y.-L. Chen, 2010: Verification on the Typhoon Morakot track and rainfall forecast issued by the Central Weather Bureau (in Chinese with English abstract). *Atmos. Sci.*, **38**, 85–98.

Yen, T.-H., C.-C. Wu, and G.-Y. Lien, 2011: Rainfall simulations of Typhoon Morakot with controlled translation speed based on EnKF data assimilation. *Terr. Atmos. Oceanic Sci.*, **22**, 647–660, https://doi.org/10.3319/TAO.2011.07.05.01(TM).

Yu, C.-K., and L.-W. Cheng, 2013: Distribution and mechanisms of orographic precipitation associated with Typhoon Morakot (2009). *J. Atmos. Sci.*, **70**, 2894–2915, https://doi.org/10.1175/JAS-D-12-0340.1.

——, and ——, 2014: Dual-Doppler-derived profiles of the southwesterly flow associated with southwest and ordinary typhoons off the southwestern coast of Taiwan. *J. Atmos. Sci.*, **71**, 3202–3222, https://doi.org/10.1175/JAS-D-13-0379.1.

Zhang, F., Y. Weng, Y.-H. Kuo, J.-S. Whitaker, and B. Xie, 2010: Predicting Typhoon Morakot's catastrophic rainfall with a convection-permitting mesoscale ensemble system. *Wea. Forecasting*, **25**, 1816–1825, https://doi.org/10.1175/2010WAF2222414.1.

——, M. Minamide, R. G. Nystrom, X. Chen, S. J. Lin, and L. M. Harris, 2019: Improving Harvey forecasts with next-generation weather satellites: Advanced hurricane analysis and prediction with assimilation of GOES-R all-sky radiances. *Bull. Amer. Meteor. Soc.*, **100**, 1217–1222, https://doi.org/10.1175/BAMS-D-18-0149.1.

Zhou, T., H.-H. Hsu, and J. Matsumoto, 2011: Summer monsoons in East Asia, Indochina and the western North Pacific. *The Global Monsoon System: Research and Forecast*, 2nd ed. C. P. Chang et al., Eds., World Scientific Series on Asia-Pacific Weather and Climate, World Scientific, 43–72, https://doi.org/10.1142/9789814343411_0004.

Zhou, Y., W. K.-M. Lau, and G. J. Huffman, 2015: Mapping TRMM TMPA into average recurrence interval for monitoring extreme precipitation events. *J. Appl. Meteor. Climatol.*, **54**, 979–995, https://doi.org/10.1175/JAMC-D-14-0269.1.

Zou, X., and Q. Xiao, 2000: Studies on the initialization and simulation of a mature hurricane using a variational bogus data assimilation scheme. *J. Atmos. Sci.*, **57**, 836–860, https://doi.org/10.1175/1520-0469(2000)057<0836:SOTIAS>2.0.CO;2.

——, W. Huang, and Q. Xiao, 1997: A user's guide to the MM5 adjoint modeling system. NCAR Tech. Note NCAR/TN-437 + 1A, MMM Division, 92 pp.